Development of a brachytherapy device for cervical cancer

in case of lower vaginal involvement or distal parametrial extension

R.C. Laan

Master of Science Thesis

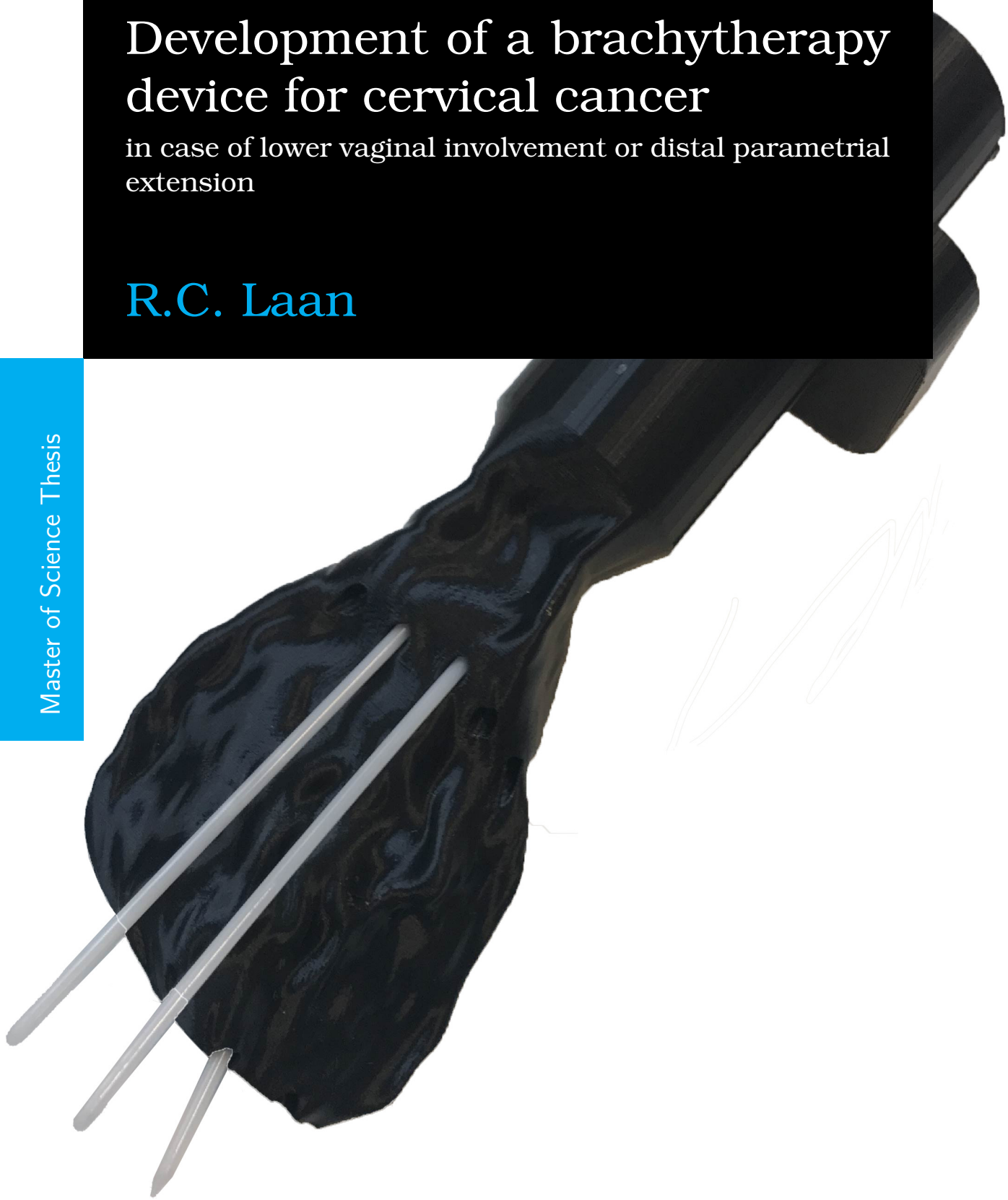

TU Delft Delft University of Technology

Department of BioMedical Engineering

Development of a brachytherapy device for cervical cancer

in case of lower vaginal involvement or distal parametrial extension

Master of Science Thesis

Supervisory team:
Dr. Ir. N. J. van de Berg
MD PhD R.A. Nout
Dr. J. J. van den Dobbelsteen
Prof.dr. J. Dankelman

R.C. Laan

August 18, 2017

Faculty of Mechanical, Maritime and Materials Engineering (3mE) · Delft University of Technology

Abstract

Brachytherapy is recommended in the treatment of cervical cancer. In case of a tumour extending lateral to the pelvic wall or more than 0.5 cm from the vaginal surface, current applicators are not sufficient to irradiate the target area. Therefore, the use of extra free-hand needles is required. Free-hand placement of interstitial needles is operator/experience dependent. The goal of this study is to develop a device that is able to irradiate the tumour in case of lower vaginal involvement or distal parametrial extension.

Based on the design criteria, a new concept has been developed. The concept is a personalised 3D-printed vaginal template with curved channels based on the MRI scan from the patient. Channel curvature constraints were examined by conducting an experiment with a separate 3D-printed template. The effects of two different needle tips (round and sharp) and 12 different curvatures (radius = 20 - 75 mm, with increments of 5 mm) on the required insertion force have been examined. A 3D-printed template with different curvatures has been suspended in a 10 m% gelatin phantom. Needles were inserted with an obturator at a speed of 5 mm/s, using a linear stage. Axial forces were measured. The data was processed and compared with a subjective user experiment of manual insertions. To examine technical feasibility of the concept, two relevant cases of cancer were used to create personalised applicators. The accuracy of the needle tip placement with these templates has been tested.

No differences have been found in maximum required insertion force for a round and sharp needle tip while passing through a template with different curvatures and while puncturing tissue. For the different curvatures, significant differences in axial force have been found for curvatures with radii $\leq$ 50 mm. Buckling behaviour occurred for radii $\leq$ 35 mm. The user experiment indicates a threshold value of 35 mm for the minimum radius for a round and sharp needle that is still comfortable to insert. Two relevant cases of vaginal cancer were successfully translated into personalised applicators. The mean accuracy of the needle tip placement was 3.9 mm. All values were $<$ 8 mm. The curvature constraints have been used to verify that the target area can be reached.

A personalised 3D-printed template with curvature constraints has been proposed as an improved method for the practice of brachytherapy in case of cervical cancer with distal parametrial extension or lower vaginal involvement. Further development and research is required to optimise the concept and verify clinical feasibility.

Table of Contents

List of Figures

List of Tables

Acknowledgements

Many people have supported me during my graduation process. This project would not have been possible without their help.

I want to thank Nick van de Berg for being a great mentor. Our weekly meetings were very useful and motivational. Your positivity helped me to become more confident.

During my graduation, I got in contact with oncologist Remi Nout from Leiden University Medical Centre. I am grateful for all the clinical input I got during our meetings and the privilege to attend a number of brachytherapy procedures. The involvement of a clinician gave this project more meaning.

I want to thank John van den Dobbelsteen and Jenny Dankelman for the opportunity to graduate at the MISIT lab with this interesting assignment and the feedback I got.

During the performance of my experiment, I got great assistance from Arjan van Dijke. I really appreciate the help and the nice work-space I got at the lab.

I want to thank my parents, Coen and Carla, for all the support throughout my years of study and reminding me to relax sometimes.

Furthermore, I want to thank the other graduate students at the lab for the support throughout the process, especially Jochem and Paulien. When I got stuck, you were there to help me or cheer me up. Thank you guys!

Chapter 1

Introduction

In 2012, there have been 528,000 new cases of cervical cancer diagnosed worldwide, with an estimated amount of 266,000 deaths.[1] The type of treatment depends on the stage of the cancer. Recommended treatment for locally advanced cervical cancer is a combination of chemotherapy and radiotherapy (combined chemoradiation) with brachytherapy.[2, 3, 4, 5] For an overview of the stages of cervical cancer and the recommended treatment, see Appendix A.

Radiotherapy Radiation therapy uses X-rays, gamma rays or charged particles to damage the DNA of a cells nucleus, with a resulting death of the cell. Death cancer cells are not able to reproduce and will be digested by the body. This results in tumour shrinkage. The amount of radiation used is measured in Gray (Gy). Gray is defined as the absorption of one joule of radiation energy per kilogram of matter.[6] There are different types of radiotherapy. A combination of brachytherapy after external beam radiation therapy (EBRT) is the standard treatment for locally advanced cervical cancer. With EBRT, x-rays are used to target the cancer from outside the body. Generally, linear accelerators are used to produce radiation.[7] The external portion of the radiotherapy to treat cervical cancer is aimed to treat the pelvic lymph nodes, parametria and primary tumour site.[3]

Brachytherapy Brachytherapy is internal radiation therapy, which involves placing a radiation source in close proximity of the cancer, using an applicator and/or hollow needles. "Brachy" is Greek for short. Brachytherapy takes advantage of the inverse-square law, where radiation dose is inversely proportional to the square of the distance from the source. Therefore, a high dose of radiation can be used to treat the gross tumour, while keeping the dose to surrounding tissue low.[3] Brachytherapy is an essential part in the treatment of advanced cervical cancer, because it is the only proven technique of providing radiation dose high enough to treat cervical cancer, without causing undue side effects to organs at risk (bladder, rectum and sigmoid).[3, 8]

Current methods In case the radioactive source is placed inside the cavity of the body with the use of an applicator, it is called intracavitary brachytherapy. In Figure 1-1 an illustration is shown from a intracavitary applicator. Intracavitary brachytherapy is the most commonly used type of brachytherapy with high control rates of 75% to 95% for smaller tumours. However, for larger tumours with parametrial extent, local control rates are lower and range between 45% and 80%.[9]

In the past, this problem has been tried to be solved by the use of interstitial implants, called interstitial brachytherapy. Since accurate free-hand implantation of needles is difficult, perineal templates have been used to improve accuracy of needle placement. A perineal template is shown in Figure 1-2a. Due to the use of transperineal templates for positioning the needles, the length between the needle insertion point and target has increased. Moreover, a high number of needles is required for optimal target coverage. This has resulted in a serious risk of late complications. In a research by Hughes et al. late bowel or bladder complications that required surgical intervention occurred in respectively 20% and 12% of the patients (n=137).[10] The same report showed a rate of 10% of patients with acute complications as bladder perforation and perineal cellulite. Furthermore, difficulties in accurate needle positioning and parallelism of the needles are reported.[4] The high amount of needles required, makes this procedure very time-consuming and labour intensive.[11] There are a few centres available with true expertise in performing interstitial brachytherapy.[12]

Due to the disadvantages and risks of interstitial brachytherapy, a novel approach has been developed: combined intracavitary/interstitial brachytherapy. Combined brachytherapy has been developed to increase the tumour coverage compared to intracavitary brachytherapy, but with a reduced chance of complications compared to interstitial brachytherapy. In Figure 1-2b the Utrecht applicator is shown. This applicator is currently used at the Leiden University Medical Centre. With this combined approach, the following aspects are tried to be achieved; (1) a greater control of needles, because the needles are shorter; (2) A lower number of needles required, because a part of the tumour can be covered by the intracavitary component.[4]

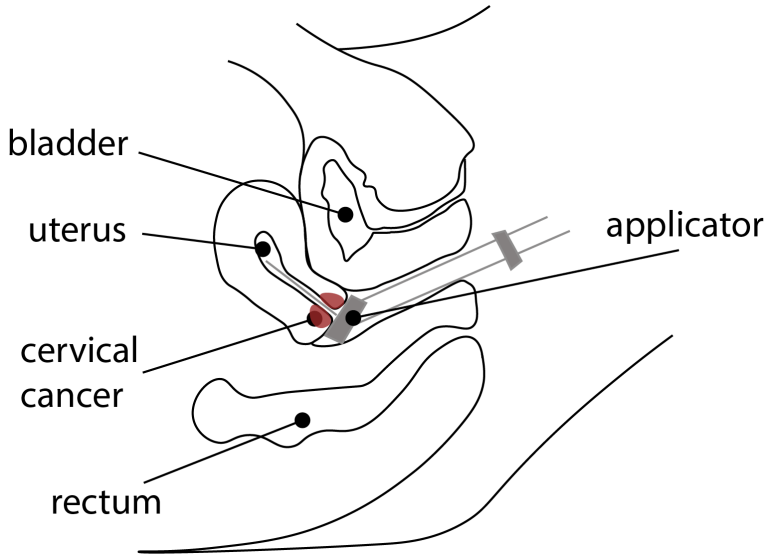

Figure 1-1: A brachytherapy applicator placed in the vaginal cavity. The applicator irradiates the cervix in close proximity.

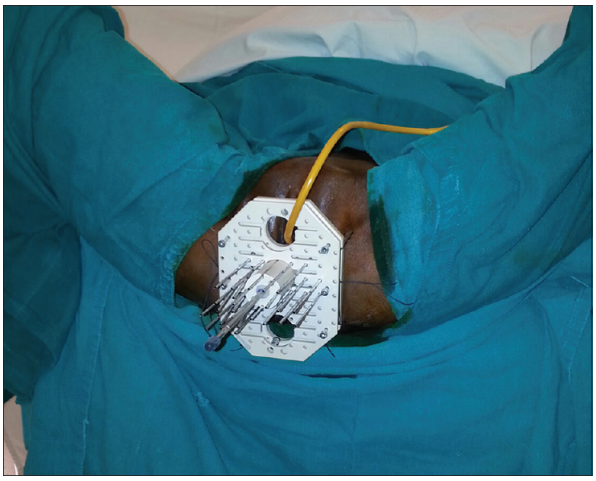

(a) Interstitial brachytherapy with the use of a transperineal template. In this case the Martinez Universal Perineal Interstitial Template is used.[13] The hole in the middle enables placement of a vaginal cylinder. A Foley catheter passes through the superior hole.

(b) The Utrecht applicator (Elekta AB, NL) that is used for combined intracavitary/interstitial brachytherapy at the LUMC. [14]

Figure 1-2: Cases of cancer where applicators are not able to properly irradiate the target area

Problem Compared to intracavitary brachytherpay, the extension of the lateral coverage of the combined approach is 10 mm.[15, 5] However, the lateral dimensions of the dosimetric reach is still limited in comparison with a perineal template.[11] According to R.A.N.[1], for cancers extending lateral to the pelvic wall or more than 0.5 cm from the vaginal surface, this combined applicator is not sufficient to cover the target area. Lower vaginal involvement usually occurs in case of recurrent cervical cancer. At the Leiden University Medical Centre (LUMC), the use of additional free-hand interstitial needles is required to reach this area. Another situation in which current applicators cannot be used, is in case of postoperative endometrial cancer. Due to scar tissue, applicators do not fit in the vaginal cavity. In Figure 1-3 these situations are shown. In Figure 1-4 the area that can not be reached is shown. The dimensions are obtained by measuring MRI scans from three tall cervical cancer patients at the LUMC. Free-hand placement of interstitial needles is operator/experience dependent. Therefore, the accuracy of needle placement and consistency during different treatments is low. In a research by Viswanathan et al. they have examined the impact brachytherapy implant quality on outcome among cervical cancer patients. They found that proper placement of the applicator results in improved disease free survival.[16] Also, multiple fractions of brachytherapy are required. Reproduction of needle positions has shown to be of most importance.[17]

Study goal The study goal is to develop a device that is able to reach the target area, shown in Figure 1-4. The target area consists of the area that is covered by available systems and the area that currently depends on free-hand catheter placement.

[1]MD PhD Remi A. Nout, Radiation Oncology, Leiden University Medical Centre, Leiden, The Netherlands

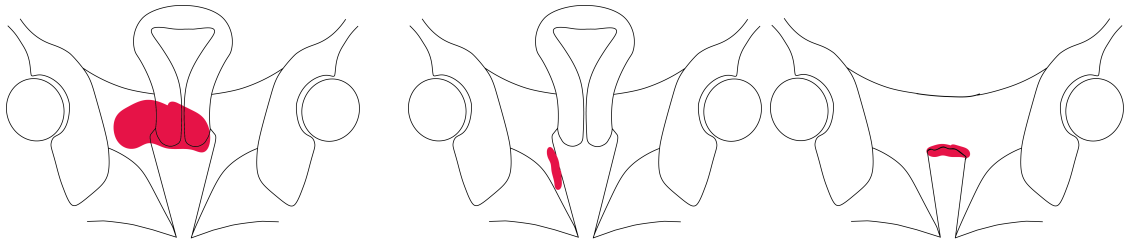

(a) Cervical cancer with distal parametrial extension

(b) Recurrent cervical cancer or vaginal cancer

(c) Postoperative endometrial cancer

Figure 1-3: Cases of cancer where current applicators are not able to properly irradiate the target area

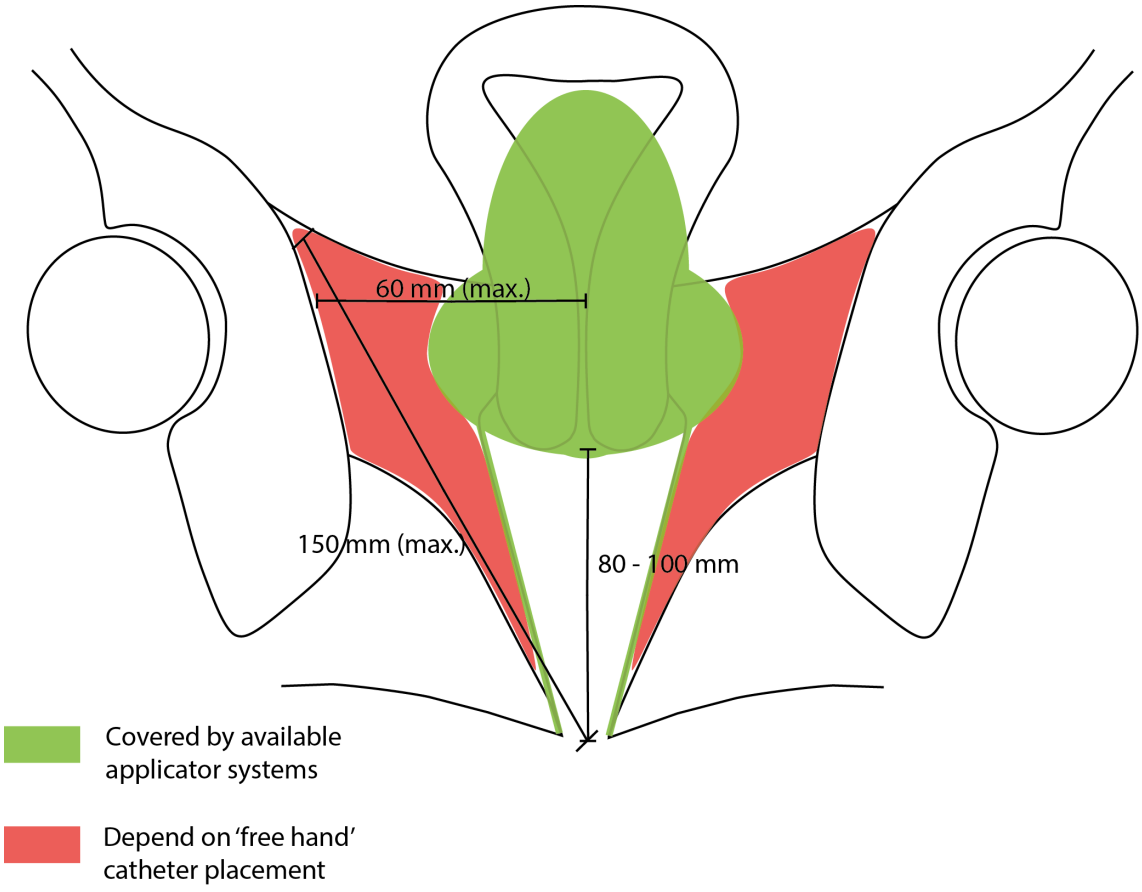

Figure 1-4: Target area of current applicators. The green area can be covered by available applicator systems. The red area depends on 'free hand' catheter placement

Chapter 2

Methods

In this chapter, the design requirements are presented. Literature research, conversations with R.A.N and a field study at the LUMC (Appendix B) have been used to formulate the design requirements. First, an overview of the current brachytherapy procedure is described to develop a better understanding of the necessary design criteria. A schematic overview of the procedure can be found in Appendix C.

2-1 Brachytherapy procedure

Based on a magnetic resonance imaging (MRI) scan or computed tomography (CT) scan, the appropriate type of applicator will be selected. The type of applicator is based on tumour geometry, location of the tumour, the patient and available techniques of the medical institute. In the operating room (OR) the applicator/needles will be placed in the vaginal cavity with ultrasound (US) guidance if necessary. Afterwards, the applicator will be fixated to prevent applicator movement. In the Leiden University Medical Centre, they use tape for fixation. An MRI scan will be taken from the pelvis with the applicator in place to visualise the tumour, surrounding organs and applicator. Using a software program (Oncentra, Elekta, SE) the tumour, applicator and surrounding organs are delineated on the MRI scan. The target area that will be irradiated will be determined and delineated. After delineation, a treatment plan will be created. This plan contains the desired places where the radioactive sources has to stop in the hollow needles (dwell positions) and the time that the source has to stay at each position (dwell times). Furthermore, the amount of times (fractions) that the patient has to be treated will be determined. The dwell positions and dwell times will be determined for each fraction. After creating the treatment plan, the patient will be brought to a special radiation room where the applicator will be attached to the afterloader, see Figure 2-1. The cables in the afterloader will be attached to the applicator and the needles. The radioactive sources are transported from the afterloader in the cables at the predefined dwell positions and dwell times. This is automatically done. After irradiation of the patient, the applicator will be removed and sterilised. [12]

Figure 2-1: The afterloader is a machine that contains cables with radioactive sources that can be inserted in the catheters of the applicator.

2-2 Design requirements

Functionality The device should provide the opportunity to insert needles in the target area. The target area of the device is shown in Figure 1-4. The target area consists of the area that is currently reached and not reached by existing applicators.

Operation The device can be manually operated by the oncologist in a user-friendly and intuitive way.

Insertion forces For the development of the device, an important quantity is the maximum allowable curvature of the needle. Ideally, the needle can be bend in a curve that (1) optimises dose distribution to cover the tumour and (2) minimises penetration length through the human tissue. In Figure 2-2 two needles with different curvatures are shown. The dose distribution is shown for the two needles with a different curvature that stop at the indicated dwell positions. It can be seen that needle I shows a better dose distribution. To minimise the amount of needles and for optimal dose distribution, the needle is placed in the longest direction of the tumour. Minimal tissue penetration can be accomplished by maximise the length through the vaginal cavity. However, the curvature of the needle is restricted by the required force to insert the needle. The surgeon has to be able to insert the needles in a controlled manner. Therefore, the insertion force cannot be too high. The relationship between curvature of the needle and required insertion force will be examined by conducting an experiment. This experiment is described in Chapter 3.

Compatibility with afterloader The device should be able to insert 6F catheters (Proguide, Nucletron BV, NL) with a 6F obturator (Proguide, Nucletron BV, NL) to enable compatibility with the afterloader device. In Section 2-1 has been described that an afterloader (Figure 2-1 is used to push the radioactive source into the needles at the dwell positions. Therefore, the device should create the opportunity to insert suitable needles. Currently, plastic needles

are used to insert the radioactive sources to enable MRI compatibility. This plastic needles are not stiff enough to penetrate the human tissue. Therefore, a stainless steel obturator is used to insert the needles. In Figure 2-3 the obturator (Proguide 6F x 294mm) and needles (Proguide 6F sharp and round) are shown that are used at Leiden University Medical Centre. Currently, sharp and round needles are available. The type of needle that is used could also have an influence on the required insertion force. Therefore, this effect is also examined in the conducted experiment that can be found in Chapter 3.

Patient suitability The device should be suitable for patients with different sized vaginal cavities. In case of postoperative gynaecological cancer, scar tissue disables proper fit of currently used applicators.

Accuracy Needle placement accuracy is important to optimise dosimetric distribution and minimise the chance of complications. According to ISO 5725-1,[18] with the term "accuracy" is intended: the closeness of a measurement to the true value. Few studies can be found to the needle placement accuracy in the practice of brachytherapy. In a pilot study to the dosimetric quality of prostate brachytherapy with customised transperineal template and interstitial plastic catheters, improved dosimetric values have been found in comparison to traditional methods. The accuracy of the placement of 100 plastic catheters tips have been analysed. The calculated mean and median catheter placement error was 2.9 mm and 2.7 mm, ranging from 0.0 mm to 5.0 mm. 91% of the errors were less than 4.0 mm. [19] These measures can be used as an indication of the desired needle accuracy.

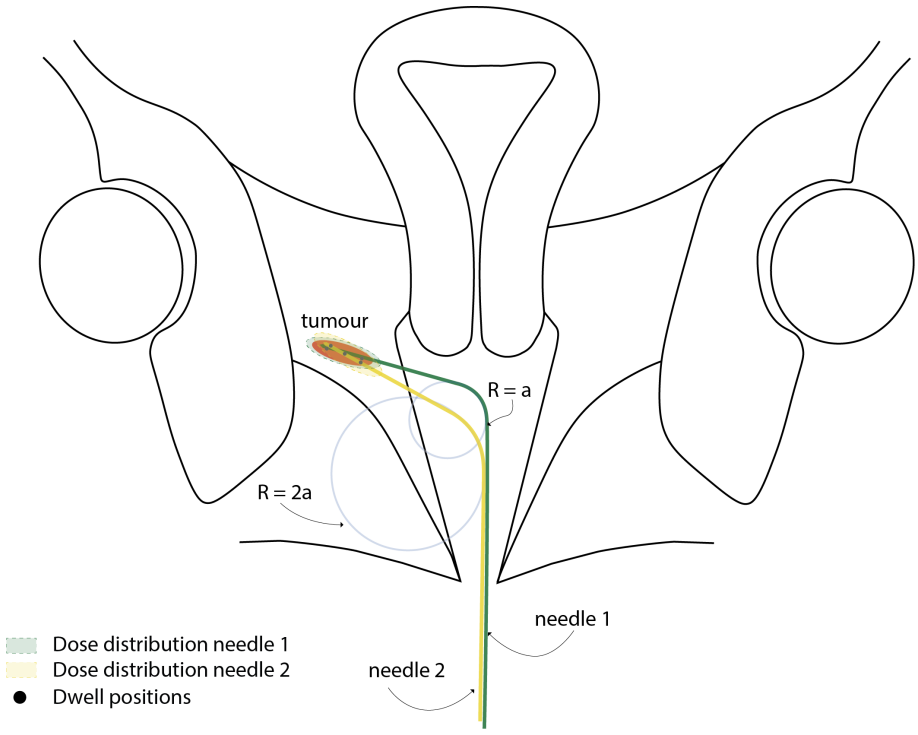

Figure 2-2: Dose distribution of two needles with different curvatures that stop at the indicated dwell positions

Sterilisation Parts have to be sterilised with available methods. With sterilisation the absolute elimination or destruction of all forms of microbial life is meant.[20] In the document "Guideline for Disinfection and Sterilisation in Healthcare Facilities, 2008" [20] available methods are described. Moreover, the geometry of the device should enable cleaning by available machines.

MRI compatibility The device should be MRI compatible. This results in a restriction in material choice. Magnetic effects can occur with chrome, steel, ferromagnetic materials and alloys.[21] Therefore, these materials are not suitable.

Safety Parts that come in contact with the patient should be non-toxic with a minimal change of tissue reactions. Therefore, the material of the device should be bio-compatible. With bio-compatible is meant:"the ability of a material to perform with an appropriate host response in a specific application"[22]

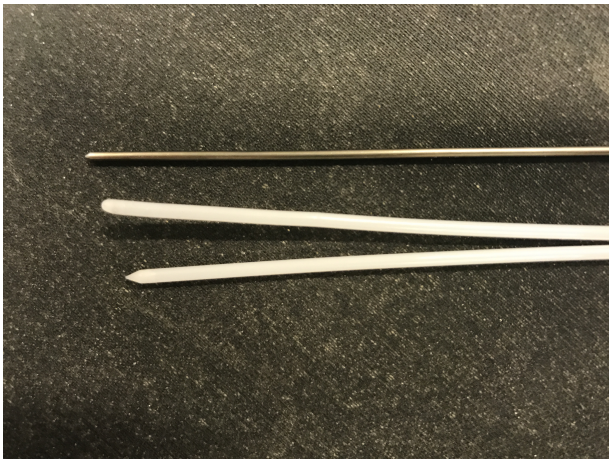

Figure 2-3: From top to bottom: an obturator to insert the needles, a round needle and a sharp needle

Table 2-1: Design requirements summary

	Criteria	Summary
1	Functionality	Able to reach the target area in Figure 1-4
2	Operation	Manually operated, user-friendly, intuitive device
3	Insertion forces	Does not exceed maximum curvature
4	Compatibility	Compatible with Proguide 6F needles and obturator
5	Patient suitability	Adjustable for different sized vaginal cavities
6	Needle accuracy	Needle placement error is < 5 mm
7	Sterilisation	Sterilizable by methods described in available guidelines [20]
8	MRI compatible	Non-magnetic material
9	Safety	Bio-compatible material

Chapter 3

Experiment: Curvature of the needle

3-1 Introduction

In the design requirements, the importance of the curvature of the needle has been explained. The limiting factor of the possible curvature is the maximum insertion force that the surgeon is able to apply. In addition, the needle tip could have an effect on the insertion force as well. The goal of this experiment is to quantify the required insertion force of a needle through different curvatures, ranging from 20-75 mm, and with different needle tips (round/sharp).

3-2 Methods and materials

To conduct the experiment, a template has been created in Solidworks (SolidWorks, Dassault Systemes, US) and printed from R05 Acrylic (P4 Standard, ENVISIONTEC INC, Germany). This print (Figure 3-1) consisted of an array of channels with path radii ranging from 20-75 mm, bridging a wall thickness of 5 mm. The insertion (axial) force in relation to current place of the needle is shown in Figure 3-2. The experiment is performed in the Minimal Invasive Surgery and Intervention Techniques (MISIT) Lab at Delft University of Technology (TU Delft).

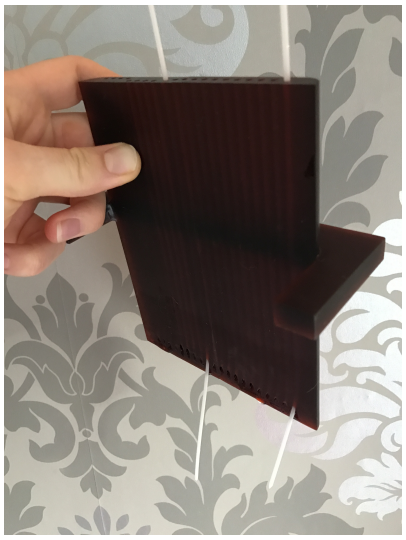

Figure 3-1: The 3D-printed array of curvatures with different radii to perform the experiment

Specimens A gelatin phantom will be used to imitate human tissue. Gelatin with a mass ratio of 10% gelatin powder and 90% water will be used. To imitate human tissue, a mass fraction between 5% and 15% can be used. The desired mass fraction depends on the type of human tissue. Cervical tissue is relatively soft. Therefore, a mass fraction of 10% has been chosen. Cervical tumour tissue is softer than healthy cervical tissue.[23] Since the maximum insertion force is the restricting factor, the stiffer healthy tissue will be taken into account. Fracture phenomena are difficult imitate with a gelatin phantom. This limitation should be taken into account.

Equipment In Figure 3-3 an overview is shown from the experimental set-up with numbers referring to the used materials with specifications in Table 3-1. The linear stage (1) is used to translate the needle with a fixed velocity in a vertical direction. A force sensor block (2) is attached to the linear stage, that contains the force sensor (3). The plastic needle was slid around the obturator. The template (6) suspended in the gelatin phantom (8) in a plastic container (7). To translate the stage in a controller manner, two manual XYZ-translation stages (10,12) were used. To attach the obturator (5) to the block (2) and to connect the XYZ-translation stages to each other and the container, coupling part were created in Solidworks and printed from PLA (Ultimaker 2 Extended+, Ultimaker, NL). In Figure 3-4 a schematic overview is shown from the input and output signals.

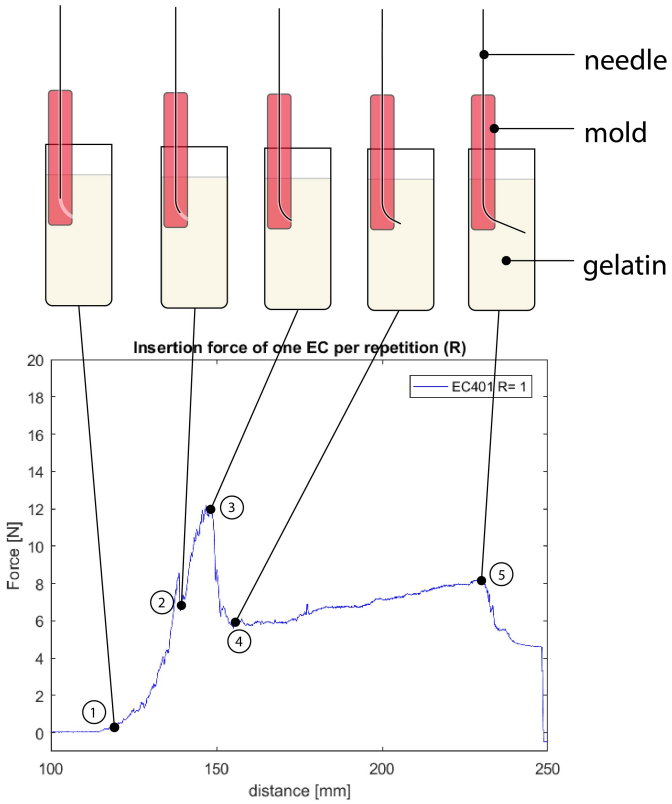

Figure 3-2: Axial reaction force on the needle tip during insertion through a curved channel

Table 3-1: Materials used in the experiment. Numbers corresponds to Figure 3-3

Nr.	Component	Manufacturer	Specifications
1	Linear stage	Aerotech, US	PRO-115
2	Force sensor block	-	
3	45N load cell	Futek, US	FLLSB200 FSH00104
4	Coupling part	-	Printed from PLA
5	Obturator + needle	Proguide, Elekta AB	6F x 294 mm obturator + 6F needle sharp/round
6	Template	DEMO, The Netherlands	Printed from R05 Acrylic
7	Plastic container	HEMA, The Netherlands	120 x 80 x 200 mm
8	Gelatin phantom	Dr. Oetker, The Netherlands	10 m% gelatin
9	Coupling part	-	Printed from PLA
10	Translation stage	Thorlabs, US	PT1/M
11	Coupling part	-	Printed from PLA
12	Translation stage	Thorlabs, US	PT1/M

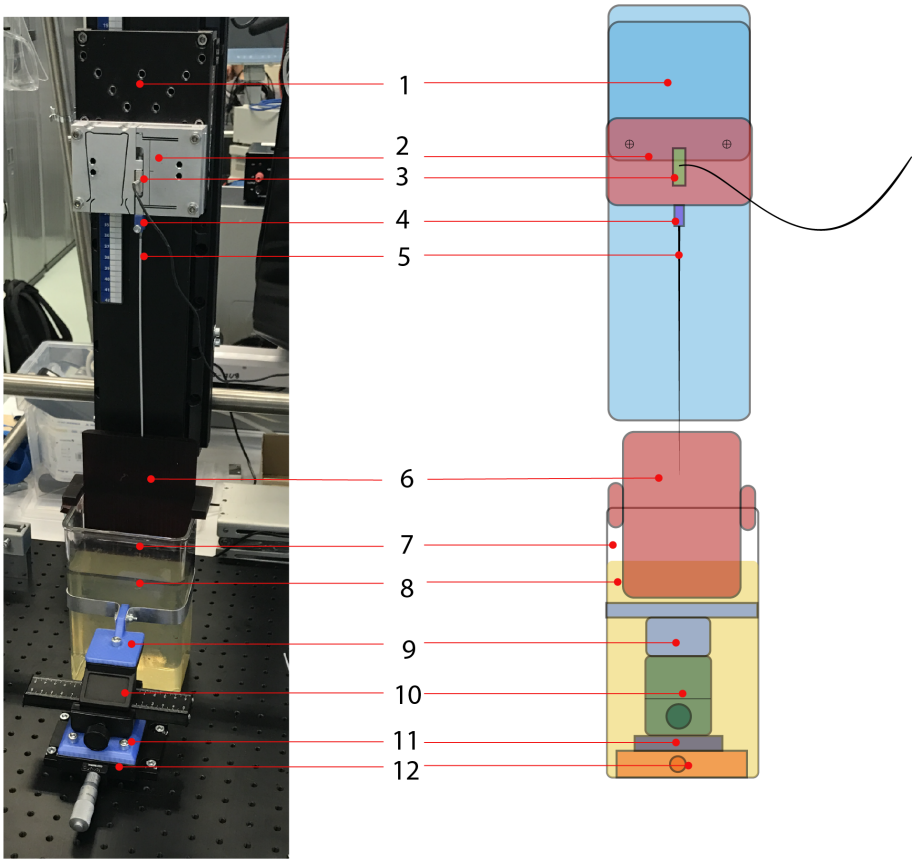

Figure 3-3: Experimental set-up. Numbers correspond to Table 3-1

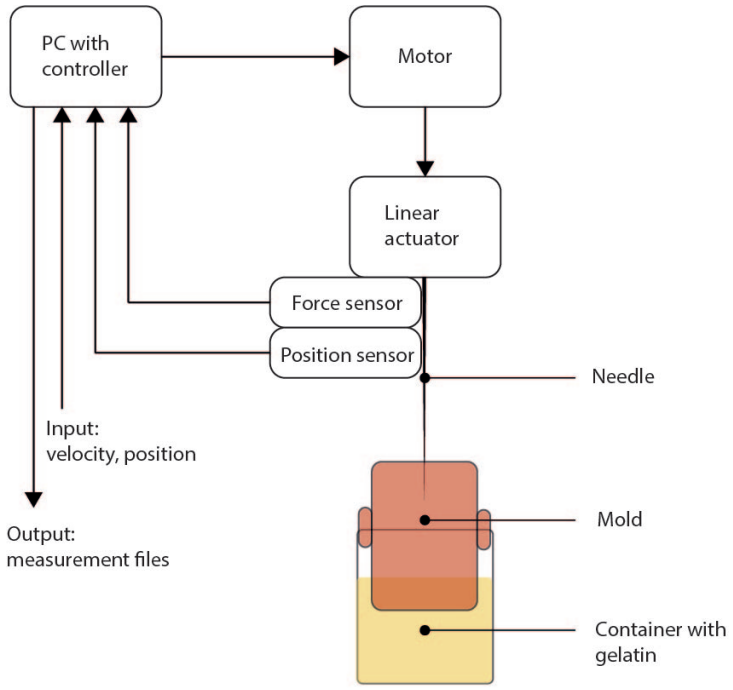

Figure 3-4: Overview of input and output signals

3-2-1 Variables

The radius of the curve and the needle tip were selected as independent variables. The axial force on the needle is the dependent variable. The wall thickness and speed of the needle do have an influence on the axial force as well. To keep the amount of independent variables manageable, these variables have been set to a fixed value. For the wall thickness a fixed value has been chosen of 5 mm. This thickness is based on vaginal geometry and is an estimation of the available space in the vagina cavity. The speed of the needle has been determined during a pilot study. An insertion speed of 5 mm/s has been chosen to be able to intervene in time in case problems occur. An overview of all variables and noise factors can be found in Table 3-2.

Radius of the needle The outgoing angle β of the needle depends on the radius of the curve R and wall thickness t, see figure 3-5. The outgoing angle is useful to test if the target are can be reached. The outgoing angle β can be calculated with the following formula:

$$\beta = \arccos \frac{R - t}{R} \tag{3-1}$$

This is can be proven as follow:

$\alpha = 90°(R \perp needle)$
$\gamma + \beta = 90°$
$\gamma + \theta = 90°$
so, $\beta = \theta = \arccos \frac{R-t}{R}$

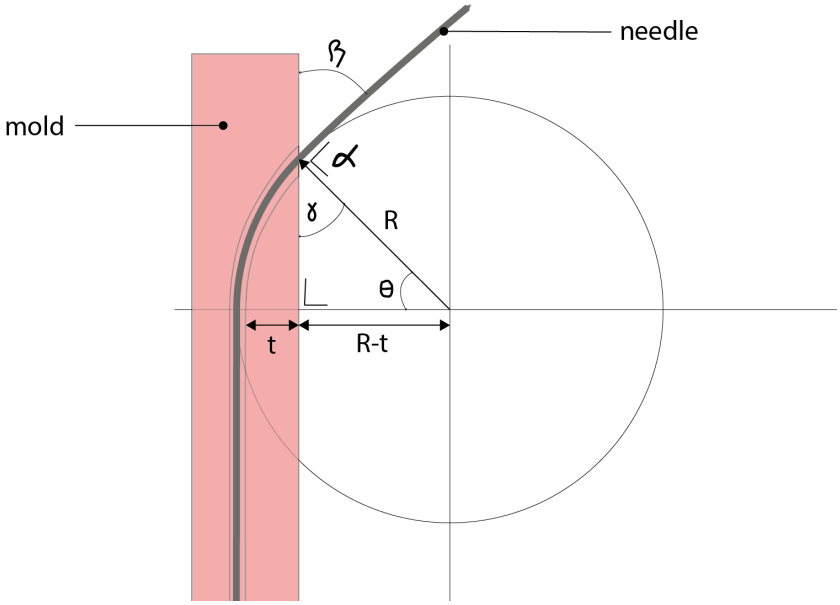

Figure 3-5: Illustration of angles to support the calculation of outgoing angle β

Table 3-2: Overview of variables

Variable	Type	Treatment	Values	Numerical values
Axial force on needle	dependent	measure	analogue	-
Radius of channel	independent	manipulate	12	20, 25, 30, 35, 40, 45, 50, 55, 60, 65, 70, 75 (mm)
Needle tip	independent	manipulate	2	round, sharp
Gelatin concentration	independent	fix		10%
Needle speed	independent	fix		5 mm/s
Temperature gelatin	independent	fix		20 degrees
Needle depth	independent	fix		230 mm
Wall thickness	independent	fix		5 mm/s
Needle wear	noise	randomise		
Accuracy needle alignment	noise	repetition		
Attention span researcher	noise	randomise		

3-2-2 Experimental design and protocol

The condition matrix with the experimental conditions (ECs) is shown in Table 3-3. Each day before conduction of the experiment, a gelatin phantom was created by mixing 1260 gr boiled water with 140 gr of gelatin powder. The template was inserted in the liquid gelatin and inserted in the fridge to cool down. The day of the experiment, the experimental set-up was prepared. Initial values were adjusted: start position = 100 (mm), speed (5 mm/s) and depth (230 mm). The force sensor was calibrated. The measurement time was set to 60 seconds. Each run the needle tip and translation stage were adjusted to meet the values of the EC. The first 10 mm of the needle was manually inserted into the channel. The needle is 294 mm long and therefore initial placement in the channel was desired. After setting initial values, the linear stage was started.

3-2-3 Data processing

Measurements were processed in Matlab (r2016b, Mathworks, US). A zero-phase moving average filter, with a kernel size of twenty, has been used to reduce noise. Figure 3-6 shows a example of the raw data and filtered data. The measured data is converted from Voltage (V) to Newton (N) (1 V = 3.1 N). Relevant measures are (2) the average force distribution for different curvatures and needle tips, (2) the maximum required insertion force, since this will be a restricting factor (point 3 in Figure 3-2) (3) the net increase of insertion force (y-value of point 4 minus the y-value of point 5 in Figure 3-2) after gelatin penetration (point 4), to examine differences in tissue penetration for a sharp and round needle. To find statistical differences, a multicomparison N-way analysis of variance is used.

Table 3-3: Condition matrix

		tip	
	n=5	**round**	**sharp**
radius	**20**	EC201	EC202
	25	EC251	EC252
	30	EC301	EC302
	35	EC351	EC352
	40	EC401	EC402
	45	EC451	EC452
	50	EC501	EC502
	55	EC551	EC552
	60	EC601	EC602
	65	EC651	EC652
	70	EC701	EC702
	75	EC751	EC752

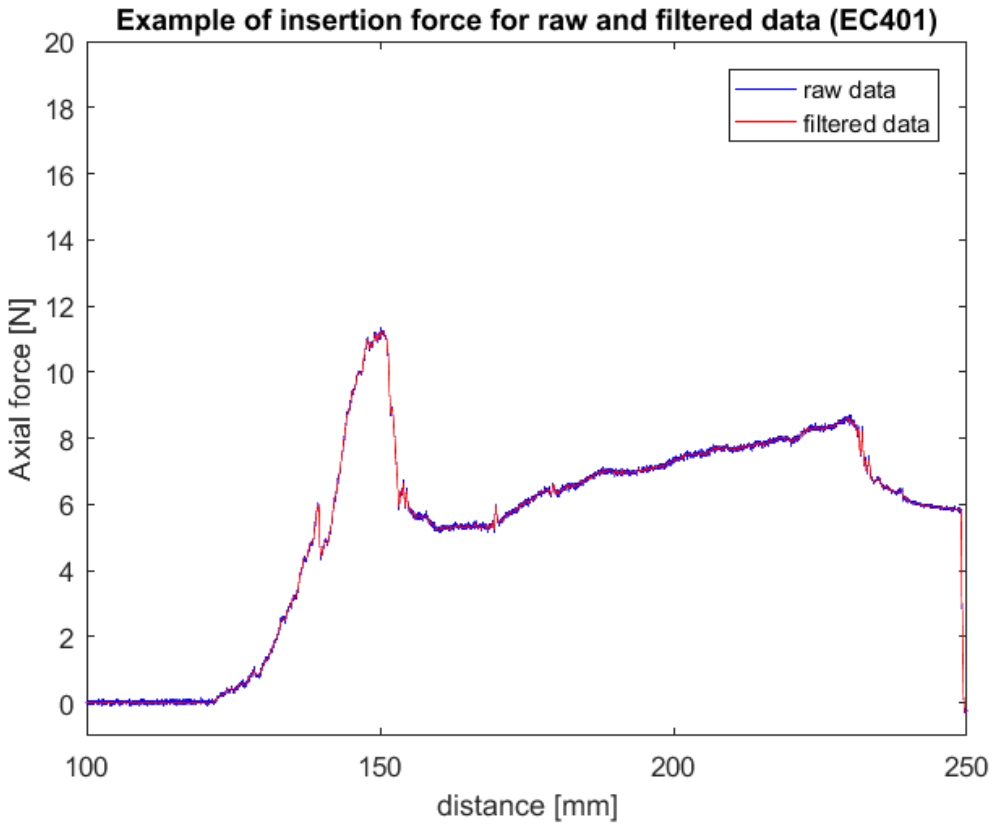

Figure 3-6: Graph with raw data and filtered data

3-3 Results

Results are obtained with Matlab. The Matlab code can be found in Appendix D.

Remarkable observations During the first run of EC201, EC202, EC251, EC252, EC301, EC302 and EC352, buckling occurred. An example of this behaviour is shown in Figure 3-7. These runs have been interrupted to avoid needle fracture. The interrupted measurements are shown in Figure 3-8. It can be seen that buckling of the needle occurs when the insertion force exceeds approximately 14 Newton. EC201, EC202, EC251, EC252 have only been measured once, since obvious buckling occurred and to prevent needle damage. EC301, EC302 have been run twice, but all runs did show needle buckling. EC352 has been performed five times, because sometimes needle buckling occurred. Since these measures have been interrupted and therefore not reliable, these runs have not been taken into account during statistical tests.

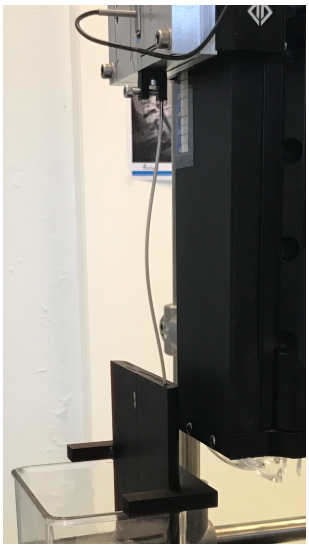

Figure 3-7: Buckling behaviour of the needle

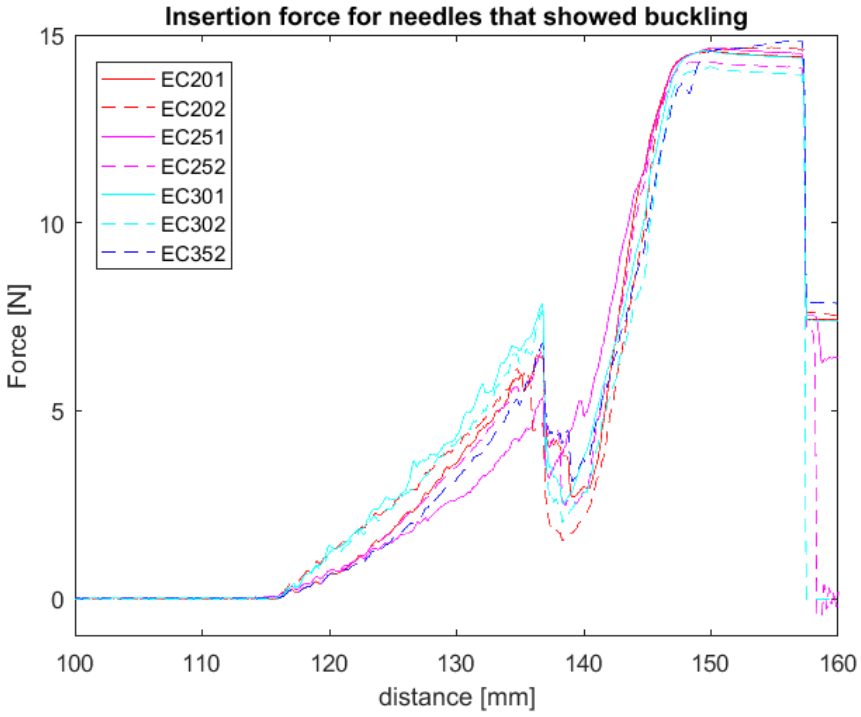

Figure 3-8: Average force distribution of interrupted runs where buckling behaviour occurred. n = 1 for EC201, EC202, EC251, EC252, n = 2 for EC301, EC302, n = 5 for EC352.

Average force distribution In Figure 3-9 the average force distribution is shown for ECs that did not show buckling behaviour. In Figure 3-9a the average force distribution is shown for a round needle tip for each radius. In Figure 3-9b the difference in average force distribution is shown between a round and a sharp needle.

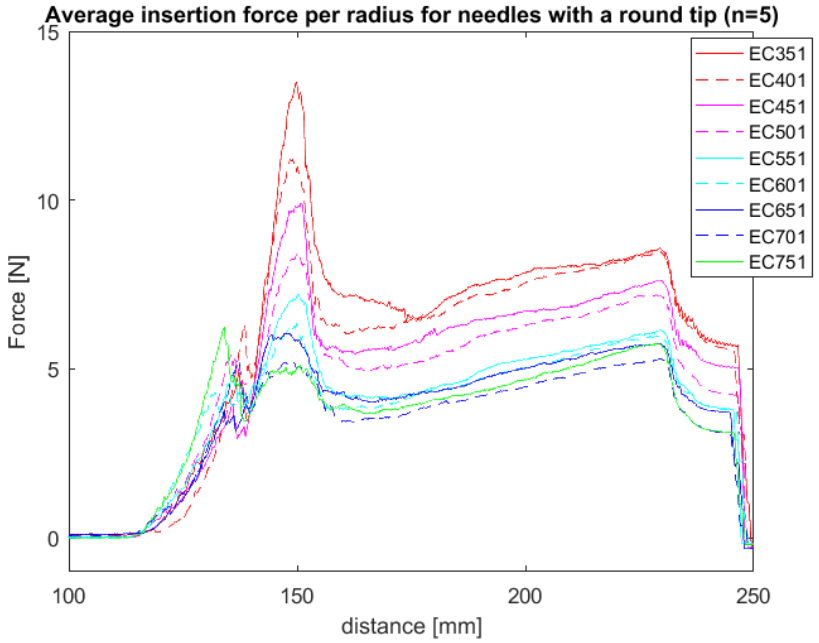

(a) Round needles Average insertion force for ECs with a round needle. n=5

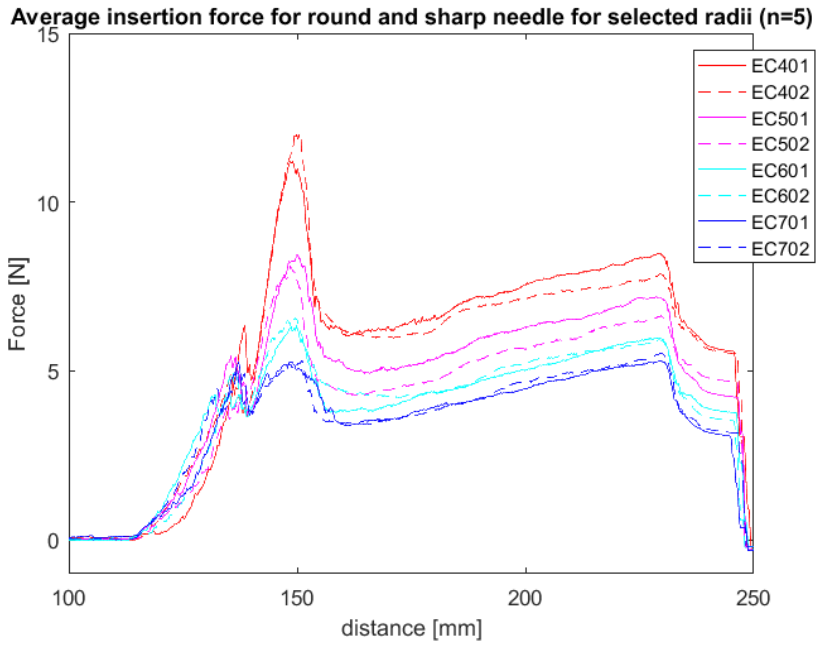

(b) Needle tips Comparison of average insertion force between needle tips for selected radii. n=5

Figure 3-9: Average insertion for per EC.

Maximum forces In Figure 3-11 a boxplot is shown from the maximum required force per EC. A multicomparison N-way ANOVA has been used to test statistical differences between each EC. The analysis is shown in Figure 3-10. Each rectangle contains ECs that are not significantly different. It can be seen that maximum forces are not different for a round and a sharp needle. For the different radii it can be seen that only for curvatures $\leq$ 50 mm a significantly higher force is required to insert the needle.

Net increase in insertion force after entering gelatin In Figure 3-12 a boxplot is shown for the increases in insertion force per EC. Both the effect of radius as the effect of the needle tip on the net increase of force are not significant (p = 0.3414 and p=0.0585 respectively).

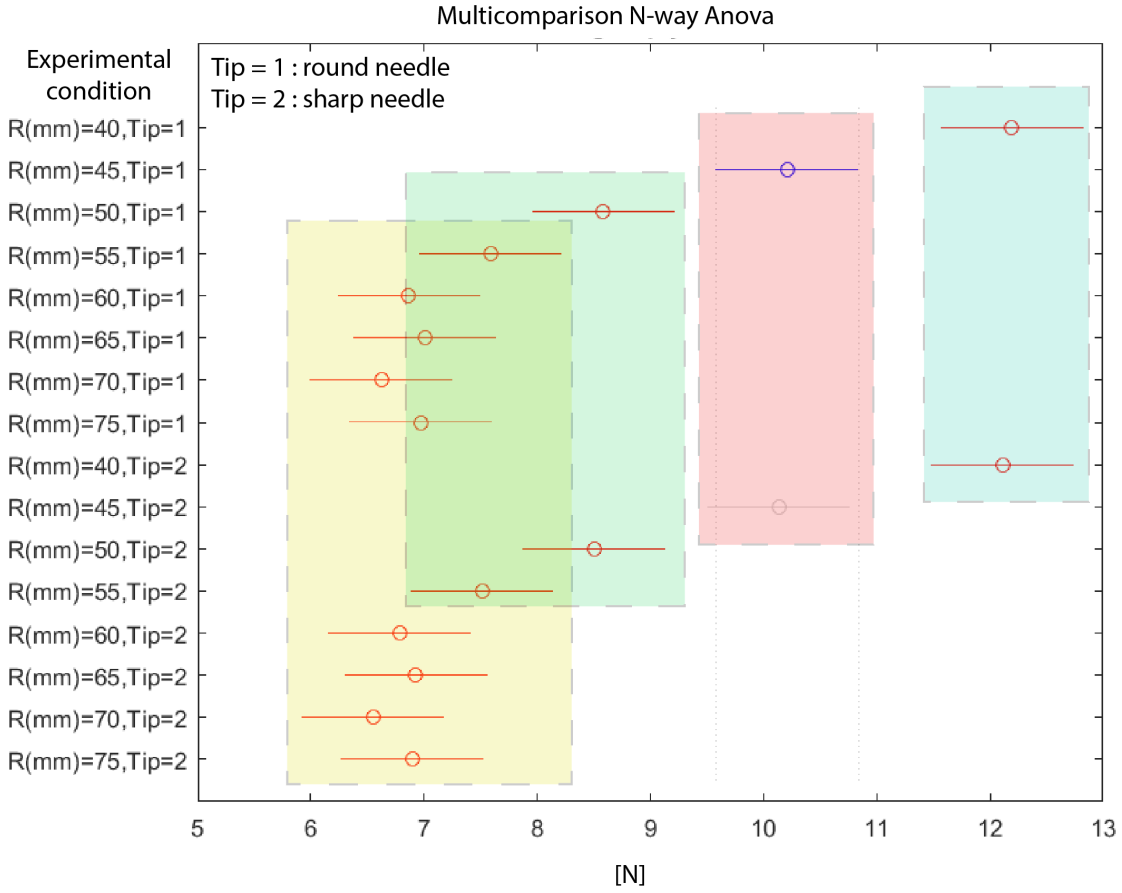

Figure 3-10: Multicomparison N-way ANOVA for the maximum required force for different radii and needle tips. Each coloured rectangular box contains ECs that are not significantly different.

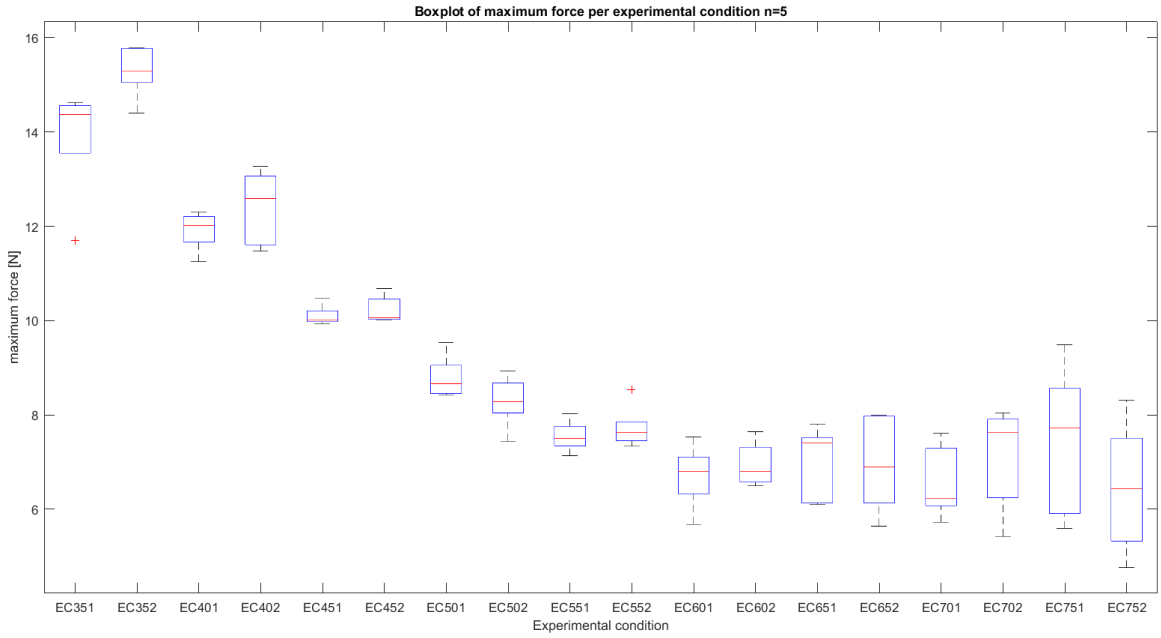

Figure 3-11: Boxplot of maximum required force per EC.

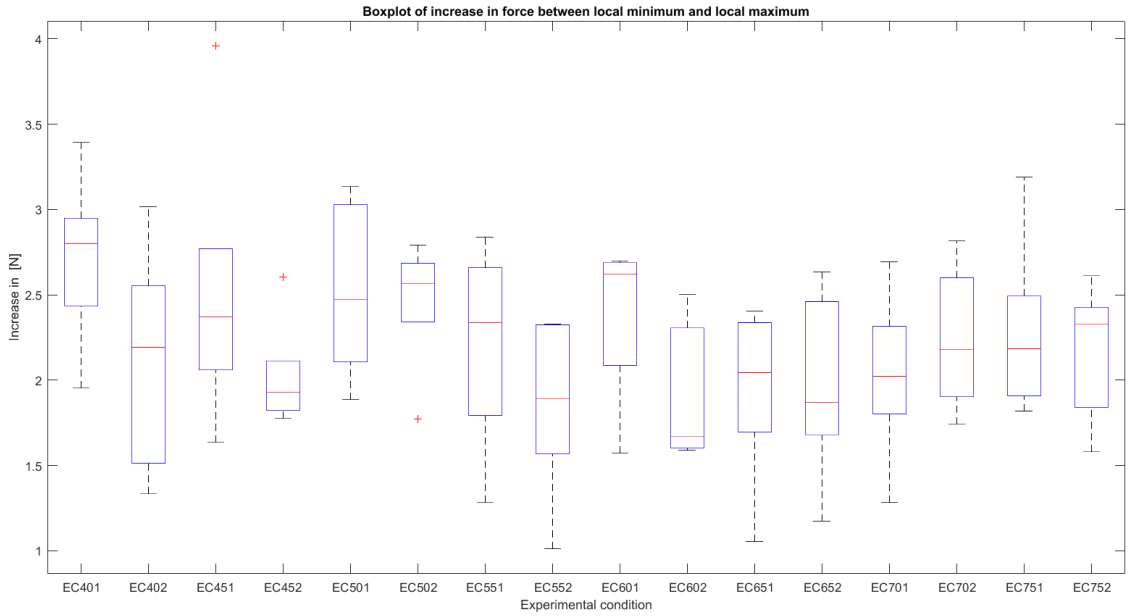

Figure 3-12: Boxplot of net increase in force after gelatin penetration per EC.

3-4 Discussion

The goal of this study was to quantify and compare the insertion force of a needle for different curvatures and needle tips. For curvatures with a radius $\leq$ 35 mm, buckling occurred. Buckling appeared when the axial force exceeds approximately 14 Newton. For radii $\leq$ 50 mm, the maximum forces for smaller radii are significantly higher than for the larger radii. For radii $\geq$ 55 mm, the differences in maximum required forces are not significant. No differences have been found between the needle tips in respect to axial forces.

An interesting observation was that buckling did occur with a sharp needle during insertion through a curvature with a radius of 35 mm in contrast with the round needle tip. This could indicate that for radii smaller than 35 mm, a difference could exists in maximum insertion force. Due to buckling, these measures could not be compared. For radii $\geq$ 55 mm, the difference in maximum required force is not significant. This corresponds with a outgoing angle β (Figure 3-5) of 25°, calculated with Eq. (3-1). For angles smaller than 25°, there is freedom in design of the template, since the differences in required forces are negligible.

With this experiment, insight in gained in the required insertion forces for different radii and needle tips. In following studies, the range of the curvatures could be reduced to find more accurate threshold values. Additionally, other factors that could have an influence on the axial forces could be examined. A factor that could reduce frictional forces is the channel diameter. Increased channel diameter could results in lower insertion forces. However, needle placement accuracy will be reduced by a larger channel diameter. Finding a balance between frictional forces and needle placement accuracy could be an interesting follow-up experiment. Other factors that could influence frictional forces are the material surface properties and printer quality. The XY-resolution printed template was 83 µm and the Z-resolution was between 25-150 µm.[24] Already, a high accuracy can be obtained. However, a smoother material surface may result in lower frictional forces.

The wall thickness and insertion speed are assumed as constant values. In reality, the wall thickness will be different for each channel, depending on the situation. Ideally, required forces can be predicted if wall thickness and radius of the channel are known. Current data can be used to estimate maximum forces for a smaller wall thickness and extrapolated for a larger wall thickness. In Appendix I a possible method is described for estimation and data extrapolation.

The insertion speed will be different per surgeon and will not be constant. To find the threshold value for a comfortable insertion of the needle, a user research could be conducted. A small user experiment has been conducted with a surgeon for a first indication of allowable insertion forces. The outcomes of this user test can be found in the next section.

Limitations of this experiment include the possible variations in the used gelatin phantoms. Needle alignment has been performed by manually operation of a translation stage. Therefore, needle alignment is susceptible for human errors. Another limitation is that initial tissue penetration in human tissue is not comparable with the initial gelatin penetration, due to differences in fracture phenomena. Initial tissue penetration would cause a higher peak value in required force than the used gelatin phantom. This would be an extra advantage of the use of a sharp needle. Organ perforation is a serious risk of the use of interstitial needles. [25, 26] The risk of organ perforation may be higher with the use of a sharp needle. Accurate

free-hand placement of needles is difficult. In case of increased needle placement accuracy, risks of organ perforation could be reduced. Therefore, the use of sharp needles could be beneficial compared to the use of round needles.

Conclusion This study has quantified required insertion forces of a round and sharp needle while passing curved channels with different radii and puncturing tissue. The outcomes can be used as reference in concept development. Follow-up studies could be useful to investigate the influence of other factors.

3-4-1 User experiment

The template is used to perform a user test with R.A.N. In this experiment a round and sharp needle have been inserted into the different channels. According this test, a radius of 35 mm is acceptable for a round and a sharp needle. With this radius, the needle can still be inserted in a controlled and comfortable manner. Coincidentally this is the same radius as the radius where the needle started to show buckling behaviour. The corresponding outgoing angle is 59°. This test can only be used as indication, since only one surgeon has been tested.

Chapter 4

Conceptual design

The final concept is a personalised 3D-printed template with channels to guide the needles to the target area. The concept consists of two parts; a personalised part for inside the vaginal cavity based on the geometry of the patient and a uniform part with slider that can be translated to the desired depth. In Figure 4-1 the concept is shown.

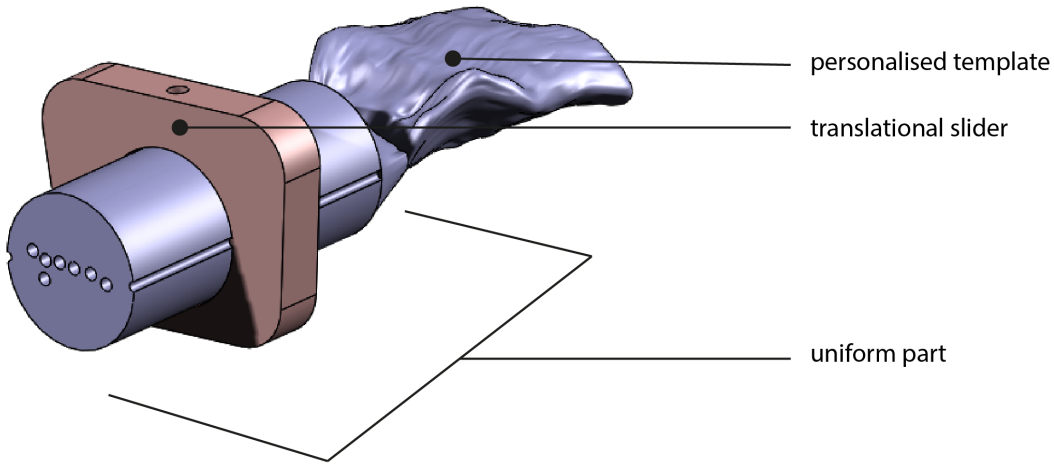

Figure 4-1: Final concept: a device that contains a personalised 3D-printed part with curved needle channels and a uniform part functions as a handhold. Fixation is possible with the slider that can be translated to the desired depth.

4-1 Personalised part

The personalised part is based on a MRI scan from the patient. The channels in the template are based on the position and geometry of the tumour. Maximum allowable curvature has to be taken into account. The process of creating a 3D printed template based on MRI images, can be divided into three stages; image acquisition, image processing and 3D printing.

Image acquisition Image acquisition is a very important step in generation of 3D objects as the quality of the object partly depends on the quality of the data. For the best results, MRI can be used. A lot of evidence exists that proves the superiority of MRI compared to CT imaging in contouring anatomy of tumours and organs, because of a better soft tissue resolution.[3, 27, 28, 29, 30, 8, 27, 31] Filling the vagina ultrasound gel allows good contrast with the surrounding structures.[32] Without regard to imaging modality, acquired data is saved in the common DICOM format (Digital Imaging and Communications in Medicine).[33]

Image processing Currently, delineation of the vaginal cavity, tumour and organs at risk is performed using the software program Oncentra (Oncentra, Elekta, SE). Oncologists can continue this delineation procedure. Subsequently, desired paths for the interstitial needles should be determined. Information of the vaginal cavity geometry and desired paths has to be translated into a printable structure, taking into account the curvature constraints. Ideally, these steps are automated. For the prototype, translation from the delineated structures into a printable file is performed manually. This process is described in Section 5.

3D printing After the desired shape of the template has been created and saved as STL-file (import format for a 3D-printer), the file can be send to the printer. The material of the template has to be suitable for 3D-printing. There are many types of 3D-printing, also known as additive manufacturing (AM). In Appendix E an overview of available methods and technologies are shown. The most commonly used AM technologies for printing plastics are Stereolithography (SLA), Fused Deposition Modelling (FDA) and Selective Laser Sintering (SLS).[34] SLA uses an UV laser to cure photopolymers. With SLS a high power laser is used to fuse small particles of e.g. a thermoplastic. FDA works by extruding a beam of a fluid thermoplastic material that immediately bonds to the layer below. These technologies vary in accuracy, surface finish, post processing requirements, costs and speed. In Table 4-1 an overview is shown from the characteristics from these technologies. FDA is the most cost-effective method. Research is required to examine if accuracy requirements can be reached with FDA. [34]

4-2 Uniform part with slider

The cylindrical uniform part is fused with the personalised part and serves as handhold during insertion of the template. The diameter of this part has to enable enough space for all channels. A smaller diameter, provides more comfort for the patient. The translational slider can be used to fixate the template at the desired depth. The notches function as navigation for the slider. The slider can be used in one rotational position only. This simplifies insertion of the template in the correct rotational orientation.

4-3 Material choice

The material of the template has to be bio-compatible, non-magnetic, sterilizable and suitable for AM. A list of the most common sterilizable materials, non-magnetic used in AM are shown in Table 4-2.[35] These materials are suitable options for the production of the device.

Table 4-1: characteristics of 3D printing technologies.[34]

	accuracy	costs	advantages	disadvantages
Stereolithography (SLA)	+++	$$	large part size	moderate strength
Selective Laser Sintering (SLS)	++	$$$	large part size, variety of materials, good strength	high cost, powdery surface
Fused Deposition Modeling (FDM)	++	$	low cost, good strength	low speed

Table 4-2: A list of materials that are bio-compatible, non-magnetic, sterilizable and suitable for 3D-printing.[35]

Material	AM method	acceptable sterilisation method
ABS M30i	FDM	Gamma irradiation, ethylene oxide
PC-ISO	FDM	Gamma irradiation, ethylene oxide
PPSF	FDM	Steam autoclave, ethylene oxide, gas plasma, chemical, gamma irradiation
Ultem	FDM	Steam autoclave
PA12 (nylon)	SLS	Steam autoclave, ethylene oxide, gas plasma, chemical, gamma irradiation

4-4 Evaluation functionality

In the design criteria it has been described that the device should provide the opportunity to insert needles in the target area.

The described concept can be evaluated with the found curvature constraints to verify if the target area can be reached. The personalised approach offers form freedom. However, curvature constraints should be taken into account. The user experiment resulted in a maximum allowable radius of 35 mm, with a wall thickness of 5 mm. This results in an outgoing angle of 31°.(3-1) In Figure 4-2 a tumour has been placed at the place that requires the sharpest angle. The length of the vaginal cavity is between 80-100 mm. The worst case scenario would be a vaginal cavity with length 80 mm and a tumour located 60 mm lateral from the mid-line. A vaginal cylinder with r=15 mm is currently used, so the maximum lateral distance can be reduced to 45 mm (60 mm - 15 mm). The corresponding outgoing angle in this case is $\alpha = \arctan \frac{45}{80}$. This results in $\alpha = 29°$. This means that in the described case, an outgoing angle of 29°is required. This means that in case curvature constraints are taken into account, the target area can still be reached. ($29° < 31°$).

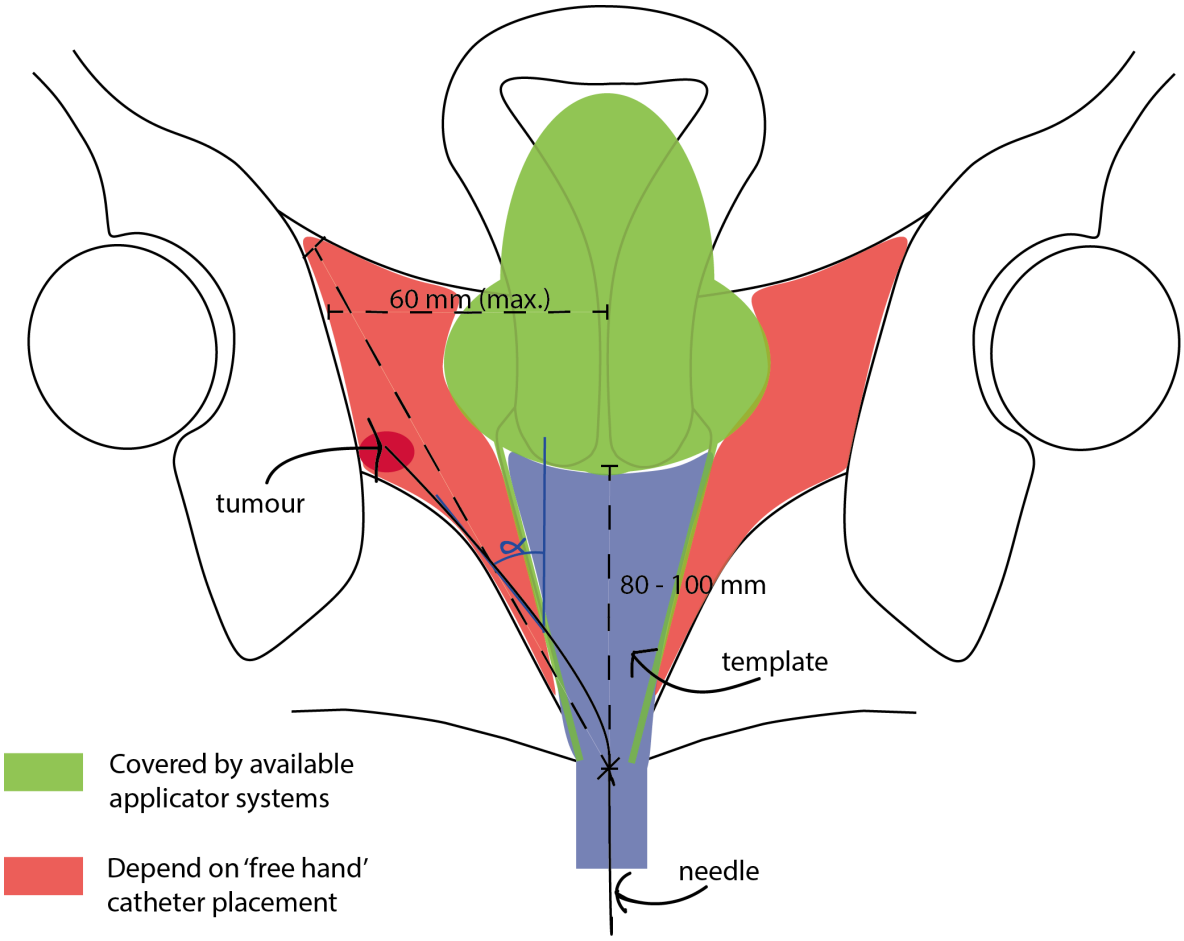

Figure 4-2: Worst case scenario

Chapter 5

Prototyping

To investigate technical feasibility, two anonymized MRI scans from patients with a relevant case of cervical cancer have been translated into personalised templates. Needle placement accuracy using these prototypes has been evaluated.

Image acquisition To create two prototypes, the contours of the vagina and desired paths of two relevant cervical cancer patients are provided in a DICOM file by R.A.N. These files contained tumour geometry as well. The images can be found in Appendix G

Data processing Several software programs have been used to translate the DICOM files into printable files;

1. **Mevislab** MeVisLab (MeVisLab, Fraunhofer MEVIS, DE) uses a modular framework for image processing with a special focus on medical imaging. In Appendix F the framework of the used modules and internal connections is shown that is used for creating the prototype. The delivered file contains information of the vaginal cavity, tumour and desired channels in world coordinates (X,Y,Z). These coordinates are separated and saved into several text-files. Each text-file contains the coordinates of the vaginal geometry of one slice. The coordinates of the desired paths were translated from circles into points, since these circles could not be processed accurately in following software programs. The points of the desired paths were saved into a text-file (.txt).
2. **Solidworks** SOLIDWORKS©3D CAD software is used for creating the template. In Figure 5-1 the steps in Solidworks are visualised. The coordinates of each slice are imported in Solidworks by the feature 'Curve Through XYZ Points'. A mesh of these curves is created by the feature "Boundary Boss/Base". Hereafter, the text-file with coordinates of the channels are imported as a point cloud. Points from corresponding channels are connected, using the feature '3D sketch'. A circle is creating at the last point of each channel at a perpendicular plane. With the feature 'Swept Cut' channels are created. The uniform part of the mesh is created in another part-file. The personalised

part and the uniform part are merged. The merged part is saved as a Stereolithography-file (STL-file). The slider is created and printed as separate part.

3. **Cura** Cura (Cura 2.6.2, Ultimaker, NL) is a software program that prepares your model for 3D printing. Cura has been used to manage printer settings.

3D printing The templates were printed from Polylactic acid (PLA) with use of the FDM printer: Ultimaker 2 Extended+ (Ultimaker, NL).

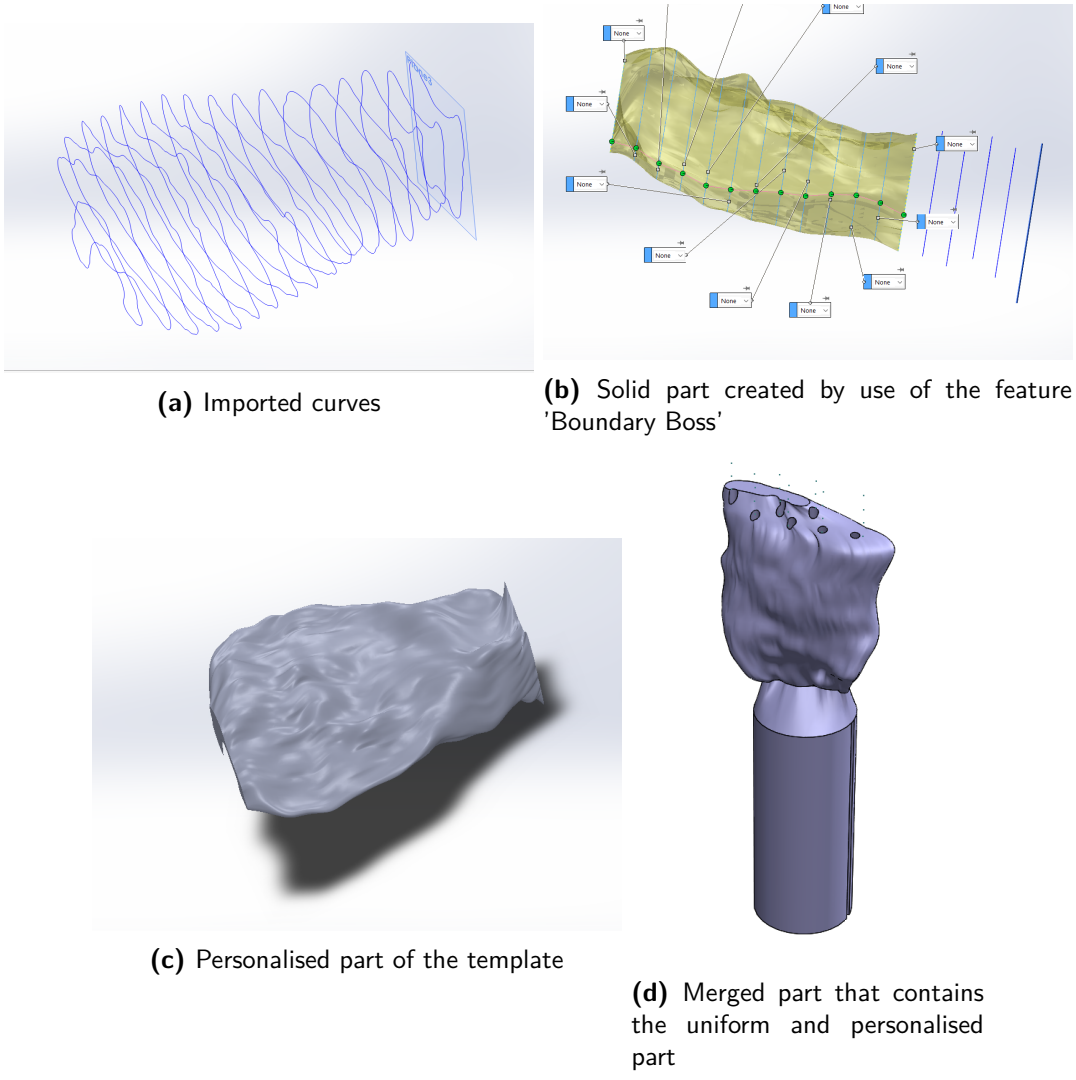

(a) Imported curves

(b) Solid part created by use of the feature 'Boundary Boss'

(c) Personalised part of the template

(d) Merged part that contains the uniform and personalised part

Figure 5-1: Steps in Solidworks

5-1 Case I

The first patient had recurring cervical cancer after radical hysterectomy. Current applicators do not properly fit, because total removal of the uterus. In Figure 5-3a the DICOM-file is shown from the vagina and desired channels. In figure Figure 5-2b the Solidworks model is shown. In figure Figure 5-2c the 3D printed vaginal template with channels is shown.

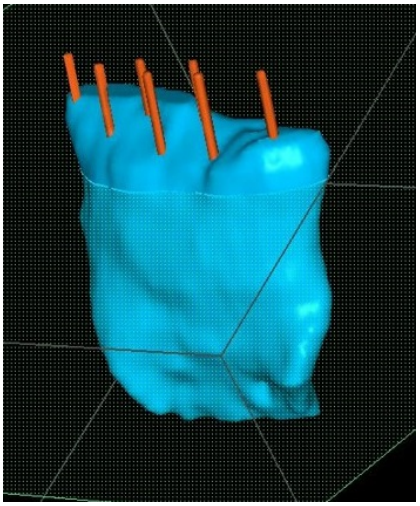

(a) RT-struct patient 2

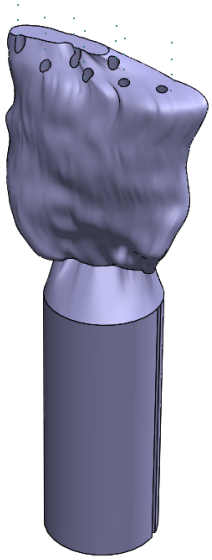

(b) Solidworks model from the template for patient 1

(c) 3D-printed mold for patient 1

Figure 5-2: Prototype patient 1

5-2 Case II

The second patient has recurring cancer in the lower vaginal area. In Figure 5-3a the DICOM-file is shown from the vagina and desired channels. In figure Figure 5-3b the Solidworks model is shown. In figure Figure 5-3c the 3D printed vaginal template with channels is shown.

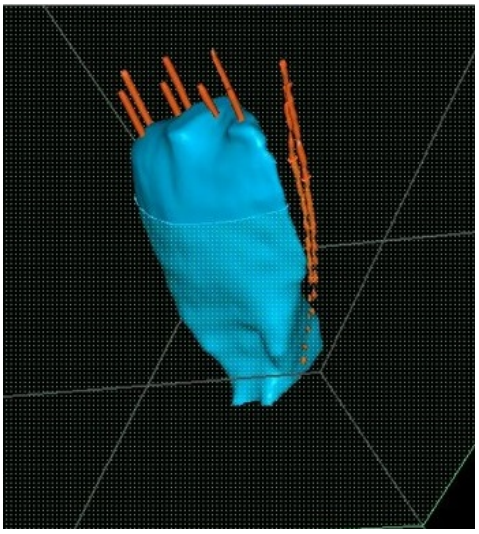

(a) RT-struct patient 2

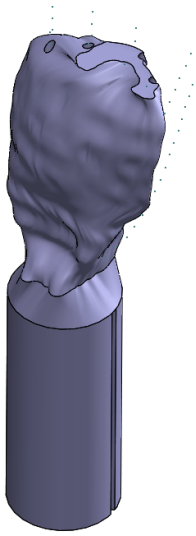

(b) Solidworks model from the template for patient 2

(c) 3D-printed mold for patient 2

Figure 5-3: Prototype patient 2

5-3 Evaluation accuracy

Set-up To evaluate the needle placement accuracy of these prototypes, a test has been performed. In Figure 5-4a the set-up is shown. The template has been fixated with four 6mm screws and a 3D-printed clamp to prevent movement, see Figure 5-4b. In Solidworks, the position of the needle tip at a distance of 150 mm of the beginning of the personalised part through each channel has been simulated and measured. A drawing has been created to translate this 3-dimensional position in a 2-dimensional drawing. By folding the drawing, the 3-dimensional position can be simulated. This distance has been based on desired target area, see Figure 1-4. This distance has been based on the worst case scenario, which is the largest dimension (150 mm) of the target area. A drawing has been created from the template with the expected position of the needle on a 1-mm grid. This drawing has been accurately positioned in relation to the template and fixated with tape.

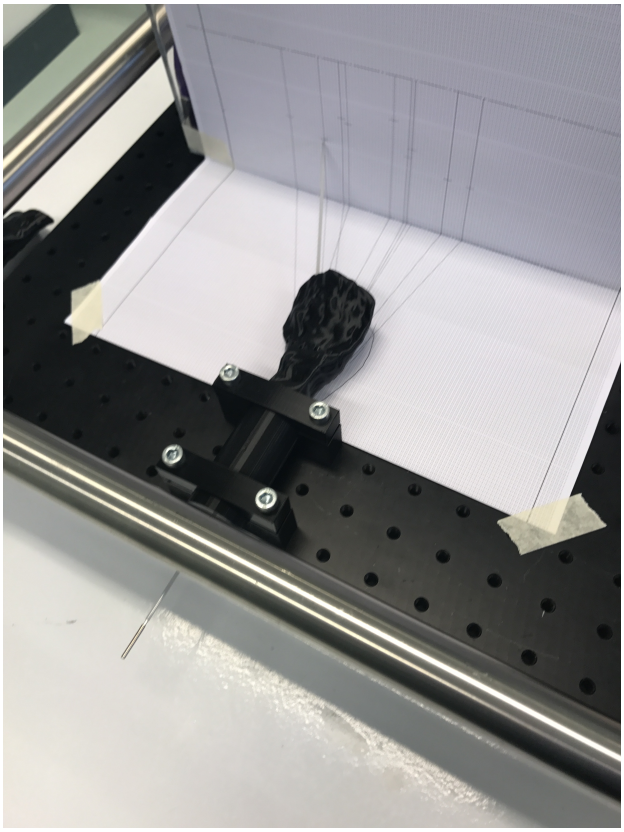

(a) Experimental set-up

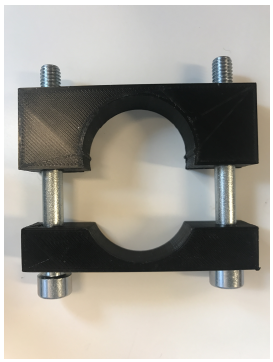

(b) printed clamp for fixation of the template

Figure 5-4: Experimental set-up

Results Each channel of prototype 1 and prototype 2 are tested two times. The results are shown in Figure 5-5. In most cases, the two measurements overlap each other and are therefore hard to distinguish in the figure. In Appendix H all measures are shown.The average deviation is 3.8 mm, with a standard deviation of 2.3 mm. The largest deviation is 8 mm. The deviations between the two measures of the same channel are all ≤ 1 mm.

5-4 Discussion

In the design criteria it has been described that the closeness of the needle tip should be < 5 mm to the expected value. The largest deviation in the accuracy test is 8 mm. Improvements are required to increase accuracy. If the results of the two measures per channel are compared to each other, it can be seen that the closeness of these measures is low ($\delta n < 1$ mm). Despite the number of repetitions is low (n=2), these results indicate a good precision.

The prototypes are created manually. More than 8 hours were used to translate the MRI scans into printable files. To reduce complexity, time and costs, automation of this process is required. Moreover, an automated process could optimise needle placement in terms of maximum dose to the target area, while minimising the dose to healthy tissue.

Furthermore, potential improvements can be obtained during image acquisition. Currently, ultrasound gel is used to visualise the vaginal cavity on the MRI scan. Ultrasound gel stays quite liquid. Therefore, gravitational forces could create a flatter visualisation of the vaginal cavity. A material that is less liquid could potentially create a more realistic image of the vaginal cavity.

In 2010, an attempt has been done to introduce a customised applicator. The template is created by pouring autopolymerized synthetic colourless resin (Palapress, Heraeus, Germany) in the vaginal cavity and let the fluid harden. Afterwards, paths are created manually by the oncologist.[36] This method is labour intensive and manually performed, and therefore prone to errors. However, the material that is used to shape the vaginal cavity could be an

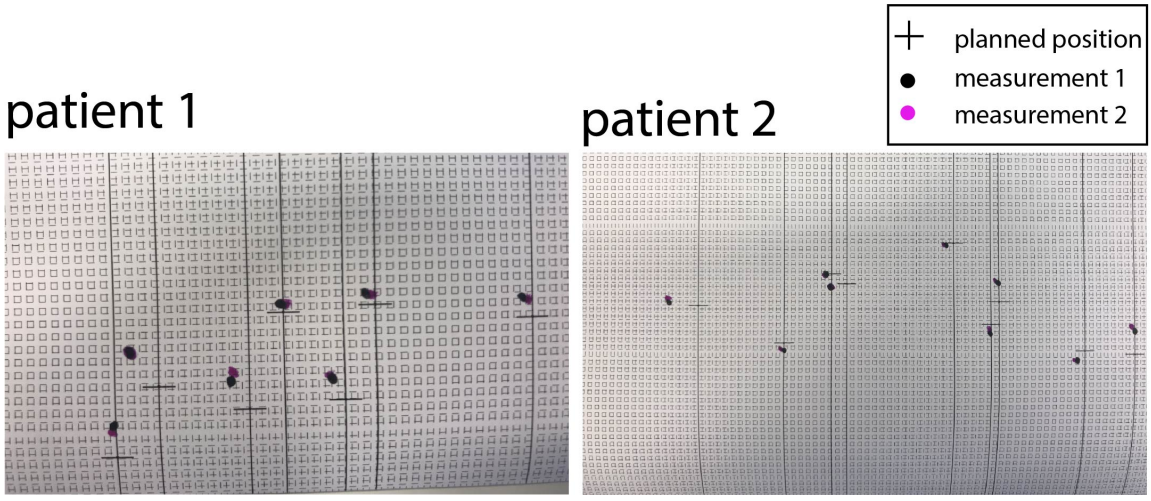

Figure 5-5: Locations of the planned needle tip position and actual needle tip position that has been measured twice.

alternative for the ultrasound gel that has been used for creating the prototypes in this paper. This material has to be adjusted to make the material visible on a MRI scan.

Another factor related to image acquisition is image quality. The 3D-printed physical models are based on imaging. Accordingly, will be prone to imaging errors. A lot of evidence exists that proves the superiority of MRI compared to CT imaging in contouring anatomy of tumours and organs, because of a better soft tissue resolution.[27, 28, 29, 8, 31] Therefore, this modality seems the best fit for creating the vaginal template. However, in-homogeneity of the magnetic field that are induced by the applicator or the patient itself, can lead to image distortions.[37] This image distortions could lead to deviations in the geometry of the vaginal template. In a research by Heerden et al., this image distortions are quantified. They have compared the actual position of an Utrecht applicator with the position on the MRI scan, using two different methods. They found displacements of < 0.4 mm and ≤ 0.8 mm respectively. Compared to displacements due to patient movement and organ deformation, the displacements caused by image distortions are small.[38]

The prototypes have been created to test technical feasibility. The personalised templates prove the feasibility of translating a MRI scan into a 3D-printed template. Evaluation of the prototypes indicates a good precision. The accuracy of the templates has to be improved to meet the design criteria.

Chapter 6

Discussion

In this study a novel concept for the practice of brachytherapy in case of cervical cancer has been presented. The concept is a personalised template with channels based on the geometry of the vaginal cavity and tumour. To investigate technical feasibility, two anonymized MRI scans from patients with a relevant case of cervical cancer have been successfully translated into a 3D-printed template. Needle placement accuracy of these prototypes is tested. The ability to reach the target area is verified, using the outcomes of the study to curvature constraints.

In Table 6-1 an overview is shown from the requirements and if additional studies are required to make a substantiated statement. The personalised approach offers the opportunity to guide channels in the desired direction. To evaluate the functionality, the curvature constraints have been used to verify whether in case of the most challenging situation, the target area can still be reached or not. The threshold value is based on a single user test. Therefore, this evaluation is can only be used as a first indication. Additional user tests are required to determine the maximum allowable insertion forces. Another design criterion that could be verified with a user study, is the user-friendliness of the device.

The prototypes are compatible with the 6F needles. This enables compatibility with the after-loader devices that are currently used to insert the radioactive sources. However, the material of the prototype does not meet all requirements. PLA is not bio-compatible.[39] However, several materials have been described that are suitable for AM, sterilizable, bio-compatible and non-magnetic. Availability, costs, surface smoothness are examples of additional factors that could be compared to find the most suitable material.

Needle placement accuracy obtained with the prototypes did not show satisfactory results. There were 5 needles (31%) that differ > 5 mm from the planned position. Presumably, these deviations were mainly due to the deviations in channel diameter and needle diameter. As already described, it is expected that a larger channel diameter results in lower frictional forces. However, needle placement accuracy will be reduced by a larger channel diameter. If other factors that are influencing the frictional forces are optimised, a smaller channel diameter could be acceptable. Another option is to make the diameter smaller at the end of the channel, so frictional forces remain low for the largest part of the channel.

Table 6-1: Design requirements summary

	Criteria	Summary	achieved
1	Functionality	Able to reach the target area in Figure 1-4	yes
2	Operation	Manually operated, user-friendly, intuitive device	t.b.d.
3	Insertion forces	Does not exceed maximum curvature	yes
4	Compatibility	Compatible with Proguide 6F needles	yes
5	Patient suitability	Adjustable for different sized vaginal cavities	yes
6	Needle accuracy	Needle placement error is < 5 mm	no
7	Sterilisation	Sterilizable by methods described in available guidelines [20]	t.b.d.
8	MRI compatible	Non-magnetic material	yes
9	Safety	Bio-compatible material	t.b.d.

A lot of literature can be found related to 3D printing of medical application. The number of medical applications for 3D printing is growing.[40] These medical applications can be categorised by organ and tissue fabrication, creation of customised prostheses, implants, anatomical models and pharmaceutical. In a study by Zein et al. they were able to print a liver based on a MRI scan of a patient for preoperative planning purposes.[41] 3D-printing in medicine is an emerging technique with a lot of potential benefits. A limitation of 3D printing could be increased time and costs spend on generation of the device. However, these costs could be compensated by reduced operation times and higher success rates of the surgical procedure. 3D- printed medical devices are expanding rapidly. It is expected that additive manufacturing will revolutionize health care.[42] Therefore, it can be expected that techniques and materials for AM are further improved and developed for the health care industry. This could indicate an enhanced feasibility of the presented concept.

Conclusion This thesis introduces a novel concept for the practice of brachytherapy in case of cervical cancer. The personalised approach shows promising results in terms of functionality, compatibility and patient suitability. Further development is required to improve the needle placement accuracy and optimise the manufacturing process and material choice. Furthermore, user studies are required to improve and test the end user experience.

Appendix A

Overview of treatment per stage

Staging Staging is a process to determine the severity of the cancer. This process is important for the selection of the right treatment. The most commonly used system for describing the stages of cervical cancer is the system designated by the Federation International de Gyneclogie et d'Obstetrique and the American Joint Committe on Cancer, also called the FIGO system.[43] This system is based on tumour size, vaginal or parametrial involvement, bladder/rectum extension and distant metastases. There are 4 main stages that are subdivided further. In table A-1 an overview is shown from the characteristics per stage.

Treatment per stage For carcinoma in situ (stage 0) surgery is most of the time sufficient to remove all abnormal tissue. For early stage disease (stage IB1 and IIA1) the main treatment types that are used are surgery, radiotherapy and combined radiotherapy with chemotherapy (concurrent chemoradiation). Preservation of fertility and the presence of lymphovascular invasion are factors taken into account. Lymphovascular invasion means that the cancer has grown into the lymph vessels. In this case, radical surgery may be required. Radiotherapy therapy and some types of surgery are not suitable for women who desire to preserve fertility. [44] For stage IB2 and locally advanced disease (stage IIA2 - IVA) the standard treatment is considered to be concurrent chemoradiation with brachytherapy.[4, 5, 44] For metastatic (stage IVB) and recurrent disease (cancer that comes back after treatment), chemotherapy is used as palliative care.[45] In case of isolated central recurrence, curative treatment can be performed with extensive surgery or radiotherapy.[46]

Table A-1: Stages of cervical cancer.

Stage	Description
0	Carcinoma in situ (preinvasive carcinoma)
I	Cervical carcinoma confined to the cervix (disregard extension to the corpus)
IA	Invasive carcinoma diagnosed only by microscopy; stromal invasion with a maximum depth of 5.0 mm measured from the base of the epithelium and a horizontal spread of 7.0 mm or less; vascular space involvement, venous or lymphatic, does not affect classification
IA1	Measured stromal invasion $\leq$ 3.0 mm in depth and $\leq$ 7.0 mm in horizontal spread
IA2	Measured stromal invasion >3.0 mm and $\leq$ 5.0 mm with a horizontal spread $\leq$ 7.0 mm
IB	Clinically visible lesion confined to the cervix or microscopic lesion greater than T1a/IA2
IB1	Clinically visible lesion $\leq$ 4.0 cm in greatest dimension
IB2	Clinically visible lesion >4.0 cm in greatest dimension
II	Cervical carcinoma invades beyond uterus but not to pelvic wall or to lower third of vagina
IIA	tumour without parametrial invasion
IIA1	Clinically visible lesion $\leq$ 4.0 cm in greatest dimension
IIA2	Clinically visible lesion >4.0 cm in greatest dimension
IIB	tumour with parametrial invasion
III	tumour extends to pelvic wall and/or involves lower third of vagina and/or causes hydronephrosis or nonfunctional kidney
IIIA	tumour involves lower third of vagina, no extension to pelvic wall
IIIB	tumour extends to pelvic wall and/or causes hydronephrosis or nonfunctional kidney
IV	tumour invades mucosa of bladder or rectum and/or extends beyond true pelvis (bullous edema is not sufficient to classify a tumour as T4)
IVA	tumour invades mucosa of bladder or rectum (bullous edema is not sufficient to classify a tumour as T4)
IVB	tumour extends beyond true pelvis

Appendix B

Field study at Leiden University Medical Centre

Meeloopdag LUMC 30/1/2017 tijdstip: 7:45 Aanwezigen: R. Nout, Rianne

Samenvatting Twee operaties bijgewoond waarin patienten werden een brachytherapy behandeling kregen met de Utrecht applicator. Na sterilisatie werd de blaas gevuld met vocht een een middel dat de zichtbaarheid op US beelden verbeterd. Dit werd gedaan met een blaascatheter. Bij patient 1 werd na verwijding van de cervix, de applicator direct ingebracht. Bij patient 2 werd gebruik van abdominale ultrasound om the applicator in te brengen. De applicator werd gefixeerd met gaas en tape. Daarna werd er een MRI scan gemaakt van de patient met de ingebrachte applicator. Vervolgens werden op deze scans de organen, tumour and applicator ingetekend. In het software programma Oncentra werd een behandelingsplan gemaakt. De gewenste posities en tijden van de radioactieve bronnen werd handmatig geoptimaliseerd door met de waardes verschillende scenario's uit te proberen. Een Excelsheet wordt gebruikt om te kijken of the stralingsdosis in het gewenste gebied hoog genoeg is en de waardens voor de omringende organen niet worden overschreden. Het behandelingsplan wordt vervolgens naar een apparaat gestuurd die de afterloader aan stuurt. De patienten werden naar een speciale kamer gebracht (met loden muren). De applicator werd aangesloten op de afterloader die automatich staalkabels met aan het uiteinde een gelaste radioactief bron door de catheters van de applicator stuurt en stopt op de verschillende posities voor een bepaalde tijd. Deze bronnen hebben een lange halveringstijd en worden elke drie maanden vervangen. Aan het eind van deze periode duurt een behandeling dus langer. Dit wordt automatisch verekend door software. Hierna ook nog een procedure bijgewoond waarin een vaginale cylinder werd ingebracht in een patient met een recidief rectumcarcinoom. Twee kleine tumours zaten aan het begin van de vagina. De cylinder bevat aparte comparimenten die apart kunnen bestralen. Nadelen van de cylinder is verhoogde kans op toxicity voor blaas en rectum.

Opvallende dingen

1. Applicator movement schijnt niet echt een probleem te zijn, wat wel in literatuur wordt aangegeven. Het gaas dat werd ingebracht om de applicator te stabiliseren en het tape dat werd gebruikt om de applicator op zijn plek te houden is een vrij simpele methode. Het duurde 5 a 10 minuten om alles goed te krijgen.

2. De blaas kan goed gereguleerd worden. Echter, de darmen is een lastig verhaal. De darmen zijn erg beweeglijk en er kan luchtophoping ontstaan. Ontluchting kan gedeeltelijk een oplossing bieden.

3. Integratie tussen Oncentra en de Excelsheet zou tijd schelen en minder gevoelig zijn voor menselijke fouten.

4. Optimalisatie van de verschillende doses per positie duurt lang en gebeurd manueel. Software is beschikbaar maar wordt niet gebruikt. De reden hiervoor is dat de software niet optimaal werkt.

5. De gevallen van laterale uitbreiding of lager vaginale tumourvorming komt vooral voor in landen waar de preventiemethodes niet zo goed ontwikkeld zijn als in Nederland.

Appendix C

Workflow

Phase	activity	Different options
Pretreatment evaluation	Imaging for diagnosis before brachytherapy treatment	CT-scan
		PET
		MRI
		X-ray
	Physical examination	
	Applicator selection	IC applicator
		IS applicator
		Combined IC/IS applicator
Applicator placement	Anesthesia	
	Physical examination	
	Placement of bladder catheter	Insert barium solution for visualization on US
		Fill bladder for stable reconstruction
	Dilation of cervix	
	Measure uterus length	
	US for visualization	
	Adjust applicator	Correct length of tandem
	Applicator placement	
	Applicator stabilization	Gauze packing
		Balloon packing
	Applicator fixation	Tape
Treatment planning	CT/MRI scan	
	Applicator reconstruction	
	Contouring	
	Make treatment plan	
Treatment	Locate patient	
	CT scan	
	Attach applicator to afterloader	
	Start treatment	
	Detach applicator from afterloader	
Repeat day after	Repeat from step Treatment – CT scan	
Repeat next fraction	Repeat from step 1	

Appendix D

Matlab code

```
clear; close all; clc
%% Find index

dt = 0.001;
sw = 145; %desired index at distance sw;
tw = (sw/5) + 0.63;
index = round(tw/dt);

%%

dt = 0.001;

slow = 190;
shigh = 230;

tlow = (slow/5) + 0.63; %from distance to time
thigh = (shigh/5) + 0.63; % from distance to time

indexlow = round(tlow/dt);
indexhigh = round(thigh/dt);
%%

for ec = 9
% Select files to analyze

%[filenames,dirname] = uigetfile('*.mat','Select data files (hold down shift or ctrl)','multiselect','on');
[filenames,dirname] = uigetfile('*.mat',['Select data files (hold down shift or ctrl)' num2str(ec)],'multiselect','on');
if ~iscell(filenames)
    filenames = {filenames}; % Ensure that "filenames" is a cell array (if there is only one file)
end
filenames = sort(filenames); % Ensure filenames are sorted in alphabetical order

% Analysis loop
pqn = length(filenames); % Total number of runs
for n = 1:pqn

    % Construct current file path
    filename = filenames{n}; % Name of i-th file
    filepath = fullfile(dirname,filename); % Construct path to file

    % A little trickery is required to load the data from the mat file into
    % a specified variable (called "data") in a neat way (without making
    % variables appear out of thin air)
    tempstruct = load(filepath); % Load variable from mat-file into temporary structure
    varnames = fieldnames(tempstruct); % Determine names of variables stored in the mat file
    run_data = tempstruct.(varnames{1}); % Assign the first field of tempstruct to the variable "data" (assuming there is only one variable in the mat file)
```

```
    % NOW you can do something with the data structure...
    C = 3.1; %Factor from Voltage to Newton
    ks = 20; %filter size voor moving average filter

    F(n,:)= (run_data.Y(1).Data)*C; %Store Force (Newton) in matrix F
    Fma(n,:)= maf(run_data.Y(1).Data,ks)*C; %Force with moving average filter
    Fmax(n,ec) = max(Fma(n,:));
    Flocalmin(n,ec) = min(Fma(n,29630:44630));%
    Flocalmax(n,ec) = max(Fma(n,40630:50000));%

    Flow(n,ec) = Fma(n,indexlow);
    Fhigh(n,ec) = Fma(n,indexhigh);
    Fratio(n,ec) = (Fhigh(n,ec)-Flow(n,ec)) / (shigh-slow);


end
    t = run_data.X.Data;
    Fmean(ec,:) = mean(Fma);
    Smean(ec,:) = std(Fma);
    Fmaxmean(ec) = max(Fmean(ec,:));
    meanFlocalmin(ec) = mean(Flocalmin(:,ec));
    meanFlocalmax(ec) = mean(Flocalmax(:,ec));

    %calculating the mean ratio
    meanRatio(ec) = mean(Fratio(:,ec));

end

%% Convert time into distance
s = (t-0.63)*5;
%%
load var
%save var.mat

%%
%% Plot of raw data
    figure
    plot(s,F,'b-'), hold on
    plot(s,Fma,'r-'),
    xlabel('distance [mm]')
    ylabel('Axial force [N]')
    title('Example of insertion force for raw and filtered data (EC401)')
    axis([100 250 -1 20])
    legend('raw data', 'filtered data')

%% Plot per EC

    plotStyle = {'b-','k-','r-','y-','m-'};

    figure
    for a = 1 : 5
    plot(s,F(a,:),plotStyle{a}), hold on
    legendInfo{a} = ['EC401 R= ' num2str(a)];
```

```
    xlabel('distance [mm]')
    ylabel('Force [N]')
    title('Insertion force of one EC per repetition (R)')
    axis([100 250 -1 20])
    end

    legend(legendInfo)
%% Plots of average values

%plotStyle = {'r-','r--','m-','m--','c-','c--','b-','b--','g-','g--','k-','k--'};
plotStyle =
{'r-','r--','w-','w-','m-','m--','w-','w-','c-','c--','w-','w-','b-','b--','w-','w-
','g-','g--'}; %plotstyle for option3


figure
%for ec = 7 : 2 : 23 %round needles
%for ec = 8 : 2 : 24 %sharp needles
for ec = [9 10 13 14 17 18 21 22] %selected radii with round and sharp needle

    %plot(s,Fmean(ec,:),plotStyle{a-6/2}), hold on
    %plot(s,Fmean(ec,:),plotStyle{a-7/2}), hold on
    plot(s,Fmean(ec,:),plotStyle{ec-8}), hold on
end
hold off
xlabel('distance [mm]')
ylabel('Force [N]')

%title('Average insertion force per radius for needles with a round tip (n=5)')
%title('Average insertion force per radius for needles with a sharp tip (n=5)')
title('Average insertion force per selected radii with a round and sharp tip
(n=5)')

axis([100 250 -1 15])

%legend('EC351','EC401','EC451','EC501','EC551','EC601','EC651','EC701','EC751')
%legend('EC352','EC402','EC452','EC502','EC552','EC602','EC652','EC702','EC752')
legend('EC401','EC402','EC501','EC502','EC601','EC602','EC701','EC702')


%% Save variables or open

%save var2.mat;
load var;

%% Plot Fmax in one plot

  labels =
{'EC201','EC202','EC251','EC252','EC301','EC302','EC351','EC352','EC401','EC402','E
C451','EC452','EC501','EC502','EC551','EC552','EC601','EC602','EC651','EC652','EC70
1','EC702','EC751','EC752'};
  plotEC(Fmax,labels), hold on
  xlabel 'Experimental condition'
```

```
  ylabel 'maximum force [N]'

%% Plot Fmax round in one plot
 Fmaxround = Fmax(:,9:2:23);

 %%
 Fmaxround = Fmax(:,7:2:23);
  labels = {'EC401','EC451','EC501','EC551','EC601','EC651','EC701','EC751'};
  plotEC(Fmaxround,labels), hold on
  xlabel 'Experimental condition'
  ylabel 'maximum force [N]'

  %% Plot Fmax sharp in one plot
  Fmaxsharp = Fmax(:,8:2:24);
  labels = {'EC402','EC452','EC502','EC552','EC602','EC652','EC702','EC752'};
  plotEC(Fmaxround,labels), hold on
  xlabel 'Experimental condition'
  ylabel 'maximum force [N]'


%% Boxplot Fmax

  labels =↙
{'EC351','EC352','EC401','EC402','EC451','EC452','EC501','EC502','EC551','EC552','E↙
C601','EC602','EC651','EC652','EC701','EC702','EC751','EC752'};
  boxplot(Fmax(:,7:24),labels)
  xlabel 'Experimental condition'
  ylabel 'maximum force [N]'
  title('Boxplot of maximum force per experimental condition n=5')
%% Plot Flocalmin in one plot

  labels =↙
{'EC401','EC402','EC451','EC452','EC501','EC502','EC551','EC552','EC601','EC602','E↙
C651','EC652','EC701','EC702','EC751','EC752'}
  plotEC(Flocalmin(:,9:24),labels)
  xlabel 'Experimental condition'
  ylabel 'Local minimum at beginning of gelatin [N]'

%% Boxplot localminimum

  labels =↙
{'EC401','EC402','EC451','EC452','EC501','EC502','EC551','EC552','EC601','EC602','E↙
C651','EC652','EC701','EC702','EC751','EC752'}
  boxplot(Flocalmin(:,9:24),labels)
  xlabel 'Experimental condition'
  ylabel 'Local minimum at beginning of gelatin [N]'
  title('Boxplot of maximum force per experimental condition n=5')
%%
for ec = 9 : 24
    for n = 1 : 5
        ratio(n, ec) = Flocalmax(n,ec) - Flocalmin(n,ec);
    end
end
```

```
  labels =↙
{'EC401','EC402','EC451','EC452','EC501','EC502','EC551','EC552','EC601','EC602','E↙
C651','EC652','EC701','EC702','EC751','EC752'}
  boxplot(ratio(:,9:24),labels)
  xlabel 'Experimental condition'
  ylabel 'Increase in  [N]'
  title('Boxplot of increase in force between local minimum and local maximum')

%%
  labels =↙
{'EC401','EC402','EC451','EC452','EC501','EC502','EC551','EC552','EC601','EC602','E↙
C651','EC652','EC701','EC702','EC751','EC752'}
  boxplot(Fratio(:,9:24),labels)
  xlabel 'Experimental condition'
  ylabel 'Increase in  [N]'
  title('Boxplot of maximum force per experimental condition n=5')

%%




%%
  labels =↙
{'EC401','EC402','EC451','EC452','EC501','EC502','EC551','EC552','EC601','EC602','E↙
C651','EC652','EC701','EC702','EC751','EC752'}
  boxplot(Ftoename(:,9:24),labels)
  xlabel 'Experimental condition'
  ylabel 'Increase in  [N]'
  title('Boxplot of maximum force per experimental condition n=5')
%% Data analysis

filename = 'anova.xlsx';
radius = xlsread(filename,'A20:A99');
tip = (xlsread(filename,'B20:B99'));
F = xlsread(filename,'C20:C99');
Fratio2 = xlsread(filename,'G20:G99');
Ftoename = xlsread(filename,'H20:H99');
%%
effect = maineffectsplot(F,{radius,tip},'varnames',{'Radius (mm)','Tip of↙
needle'});
legend('1 = Round, 2 = sharp')
title('effects plot')
%%
effect2 = multivarichart(F,{radius,tip},'varnames',{'Radius (mm)','Tip of↙
needle'});
legend('1 = Round', '2 = sharp')
title('effects plot')
ylabel = 'maximum insertion force'

%%
p = anovan(F,{radius, tip},'varnames',{'Radius (mm)','Tip of needle'});
```

```
%%
[~,~,stats] = anovan(F,{radius, tip},'varnames',{'Radius (mm)','Tip of needle'});
%%
results = multcompare(stats,'Dimension',[1 2])

%%

results = multcompare(stats);

%% sharp needle goes faster through gelatin

%%
[~,~,stats2] = anovan(Fratio,{radius, tip},'varnames',{'Radius (mm)','Tip of
needle'});
%%
[~,~,stats3] = anovan(Ftoename,{radius, tip},'varnames',{'Radius (mm)','Tip of
needle'});
%%
results = multcompare(stats3,'Dimension',[1 2])

%%
effect2 = multivarichart(Ftoename,{radius,tip},'varnames',{'Radius (mm)','Tip of
needle'});
legend('1 = round needle', '2 = sharp needle')
title('Increase in force after entering gelatin [N]')

%%
effect2 = multivarichart(Fratio2,{radius,tip},'varnames',{'Radius (mm)','Tip of
needle'});
legend('1 = round needle', '2 = sharp needle')
title('Increase in force after entering gelatin [N]')

%%
[~,~,stats3] = anovan(Ftoename,{radius, tip},'varnames',{'Radius (mm)','Tip of
needle'});
results = multcompare(stats3,'Dimension',[1 2])
```

Appendix E

Additive Manufacturing Technologies: An Overview

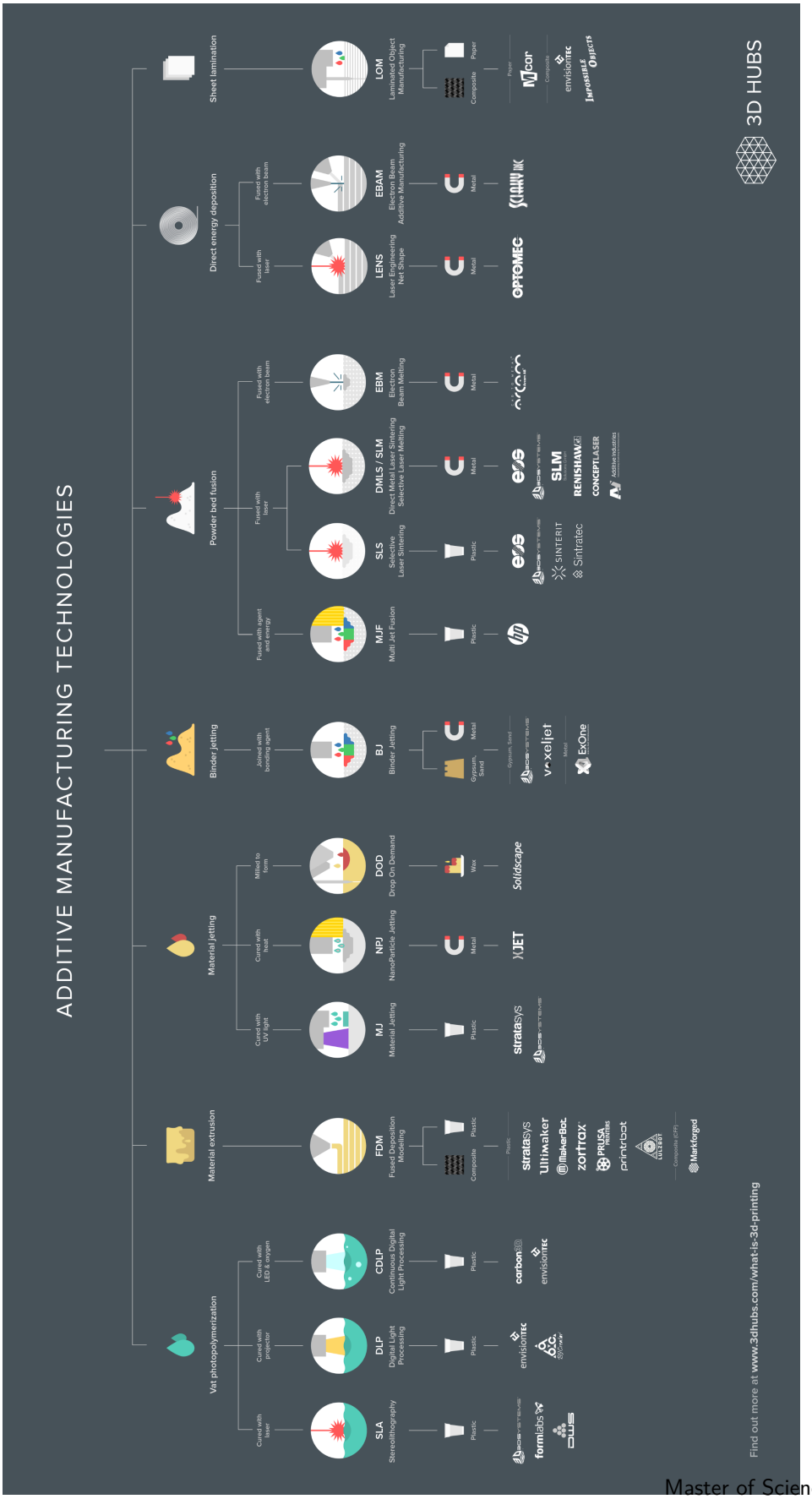
ADDITIVE MANUFACTURING TECHNOLOGIES
Vat photopolymerization
Material extrusion
Material jetting
Binder jetting
Powder bed fusion
Direct energy deposition
Sheet lamination
SLA
Stereolithography
DLP
Digital Light Processing
CDLP
Continuous Digital Light Processing
FDM
Fused Deposition Modeling
MJ
Material Jetting
NPJ
NanoParticle Jetting
DOD
Drop On Demand
BJ
Binder Jetting
MJF
Multi Jet Fusion
SLS
Selective Laser Sintering
DMLS / SLM
Direct Metal Laser Sintering
Selective Laser Melting
EBM
Electron Beam Melting
LENS
Laser Engineering Net Shape
EBAM
Electron Beam Additive Manufacturing
LOM
Laminated Object Manufacturing
Find out more at www.3dhubs.com/what-is-3d-printing
3D HUBS

Figure E-1: [47]

Appendix F

Detailed description of prototype

MeVisLab [**?**] uses a modular framework for image processing with a special focus on medical imaging. In Figure F-1 the framework of used modules and internal connections is shown that is used for creating the prototype.

1. **DirectDicomImport** Import RTstruct into the document
2. **RTstruct To ML** This module converts the object to ML (MeVis Image Processing Library) structures to enable further processing.
3. **CSO Manager** This module is used to separate the coordinates of the different structures (vaginal cavity, tumour, channels) per slice of the MRI scan.
4. **CSOFreehandProcessor** Each slice contains several circles with diameter of 2 mm as indication for the desired channels. In each circle a point is drawn. These points can be saved as world-coordinates. In this module the settings for manual drawing in the MRI scan can be adjusted. For Creation Mode, the option "Point" is chosen.
5. **Panel View2D** In this module points can be drawn on each slice.
6. **CSO Manager** The coordinates from the vagina and circles have be deleted, except the created points. Therefore, the CSO Manager is used for the second time.
7. **CSOConvertToXMarkerlist** The path points that are created in the Panel View2D are converted into worldcoordinates.
8. **XMarkerListToFile** The coordinates are saved into a text-file.

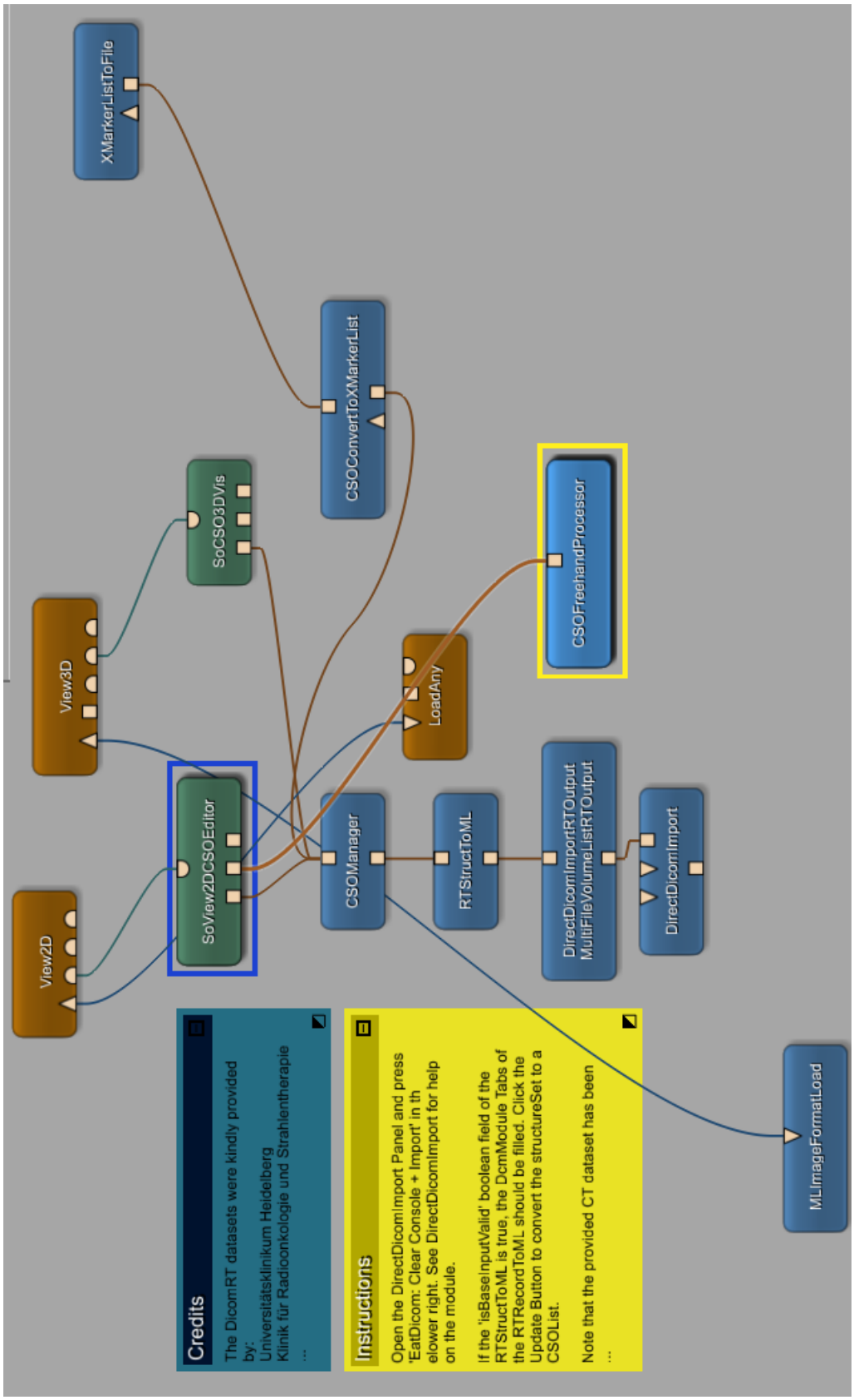

Figure F-1: Overview of modular framework

Appendix G

DICOM files

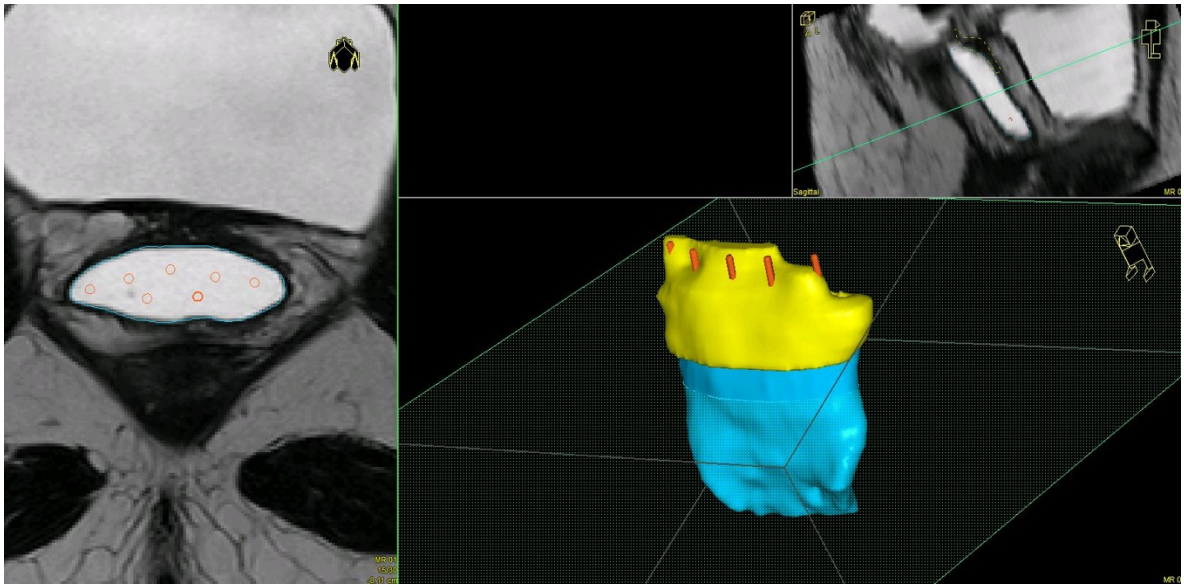

Figure G-1: RTstruct Patient 1

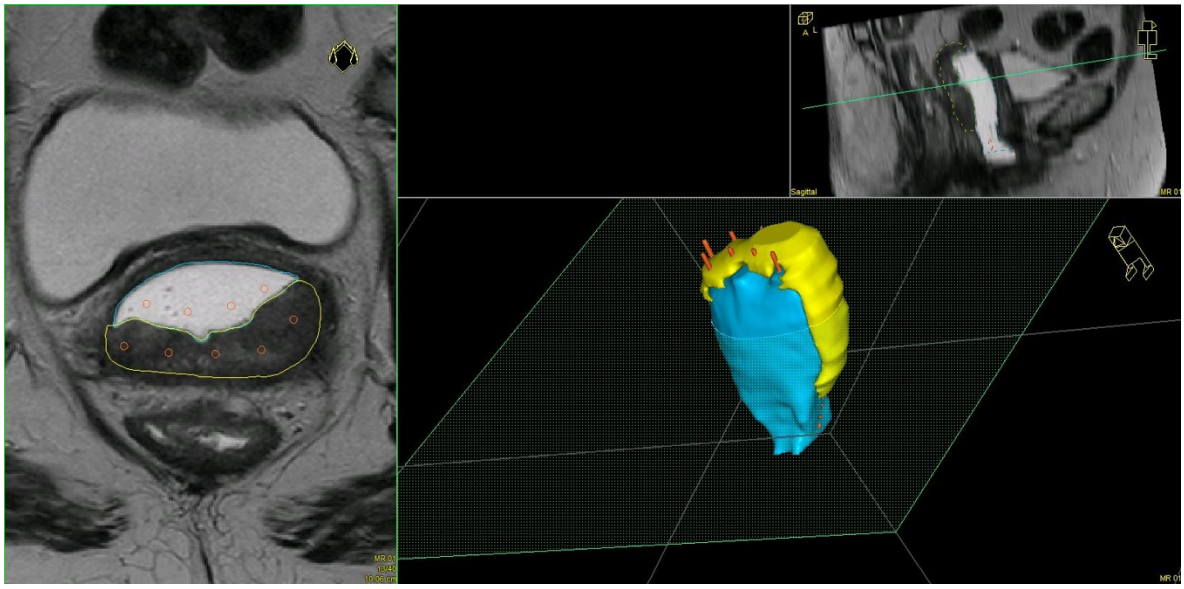

Figure G-2: RTstruct Patient 2

Appendix H

Accuracy results in detail

In Table H-1 and Table H-2 the deviations are listed per prototype. The total mean and standard deviations per prototype and in total are shown in Table H-3.

Table H-1: Deviation of the planned needle tip position of each needle in the template of case I with the actual needle position. The actual needle tip position is measured two times (n1, n2). The difference between these measured is displayed as δn

Patient 1, n = 2			
needle	n1 (mm)	n2 (mm)	δn (mm)
1	5	4	1
2	6	6	0
3	5	6	1
4	1	1	0
5	3	4	1
6	2	1	1
7	3	3	1

Table H-2: Deviation of the planned needle tip position of each needle in the template of case II with the actual needle position. The actual needle tip position is measured two times (n1, n2). The difference between these measured is displayed as δn

Patient 2, n = 2			
needle	n1 (mm)	n2 (mm)	δn (mm)
1	8	8	1
2	2	1	1
3	1	1	0
4	5	5	0
5	2	2	0
6	2	1	1
7	5	6	1
8	3	4	1
9	6	7	1

Table H-3: Mean and standard deviation (std) of the deviation of the real needle placement in comparison with the planned needle templates both templates (mm)

Template 1	Mean	3,57
	Std	1,87
Template 2	Mean	4,05
	std	2,59
Total	Mean	3,85
	Std	2,29

Appendix I

Possible method for data extrapolation

The data of the curvature experiment could be used to estimate the maximum axial force in case of a smaller wall thickness. In Figure I-1 the data cursor is at the point x = 147 mm. The peak value for 5 mm is at a distance of 149 mm. If the wall thickness was 3 mm, instead of 5 mm, the peak would occur at approximately 147 mm. The corresponding y-value is in this case 10.39 Newton. If a relation could be found between wall thickness and peak value, data could be extrapolated for a larger wall thickness as well. To verify this method, an experiment could be conducted.

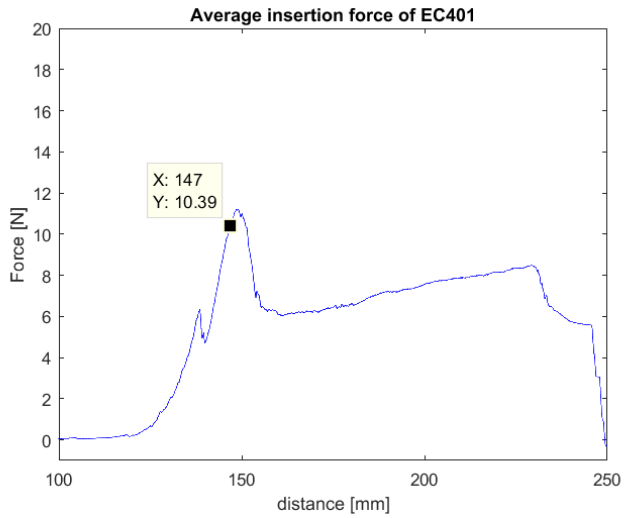

Figure I-1: Graph of axial force on the needle with datacursor at x=147 mm. This is the estimated peak force for a wall thickness of 3 mm.

Bibliography

[1] World Health Organization. Estimated incidence, mortality and prevalence worldwide in 2012. http://globocan.iarc.fr/old/FactSheets/cancers, 2012. accessed 2016-10-12.

[2] John A Vargo and Sushil Beriwal. Image-based brachytherapy for cervical cancer. *World journal of clinical oncology*, 5(5):921, 2014.

[3] Robyn Banerjee and Mitchell Kamrava. Brachytherapy in the treatment of cervical cancer: a review. *Int J Womens Health*, 6:555–64, 2014.

[4] Johannes CA Dimopoulos, Christian Kirisits, Primoz Petric, Petra Georg, Stefan Lang, Daniel Berger, and Richard Pötter. The vienna applicator for combined intracavitary and interstitial brachytherapy of cervical cancer: clinical feasibility and preliminary results. *International Journal of Radiation Oncology* Biology* Physics*, 66(1):83–90, 2006.

[5] Christian Kirisits, Stefan Lang, Johannes Dimopoulos, Daniel Berger, Dietmar Georg, and Richard Pötter. The vienna applicator for combined intracavitary and interstitial brachytherapy of cervical cancer: design, application, treatment planning, and dosimetric results. *International Journal of Radiation Oncology* Biology* Physics*, 65(2):624–630, 2006.

[6] International Bureau of Weights, Measures, Barry N Taylor, and Ambler Thompson. The international system of units (si). 2001.

[7] American Cancer Society. Surgery for cervical cancer. http://www.cancer.org/cancer/cervicalcancer, 2016. accessed 05/11/2016.

[8] Matthew M Harkenrider, Fiori Alite, Scott R Silva, and William Small. Image-based brachytherapy for the treatment of cervical cancer. *International Journal of Radiation Oncology* Biology* Physics*, 92(4):921–934, 2015.

[9] Alain Gerbaulet and Alain Gerbaulet. The gec estro handbook of brachytherapy. 2002.

[10] Luke Hughes-Davies, Barbara Silver, and Daniel S Kapp. Parametrial interstitial brachytherapy for advanced or recurrent pelvic malignancy: the harvard/stanford experience. *Gynecologic oncology*, 58(1):24–27, 1995.

[11] Takahiro Oike, Tatsuya Ohno, Shin-ei Noda, Hiroki Kiyohara, Ken Ando, Kei Shibuya, Tomoaki Tamaki, Yosuke Takakusagi, Hiro Sato, and Takashi Nakano. Can combined intracavitary/interstitial approach be an alternative to interstitial brachytherapy with the martinez universal perineal interstitial template (mupit) in computed tomography-guided adaptive brachytherapy for bulky and/or irregularly shaped gynecological tumors? *Radiation Oncology*, 9(1):1, 2014.

[12] Akila N Viswanathan, Bruce Thomadsen, American Brachytherapy Society Cervical Cancer Recommendations Committee, et al. American brachytherapy society consensus guidelines for locally advanced carcinoma of the cervix. part i: general principles. *Brachytherapy*, 11(1):33–46, 2012.

[13] Alvaro Martinez, Richard S Cox, and Gregory K Edmundson. A multiple-site perineal applicator (mupit) for treatment of prostatic, anorectal, and gynecologic malignancies. *International Journal of Radiation Oncology* Biology* Physics*, 10(2):297–305, 1984.

[14] Christel N Nomden, Astrid AC de Leeuw, Marinus A Moerland, Judith M Roesink, Robbert JHA Tersteeg, and Ina Maria Jürgenliemk-Schulz. Clinical use of the utrecht applicator for combined intracavitary/interstitial brachytherapy treatment in locally advanced cervical cancer. *International Journal of Radiation Oncology* Biology* Physics*, 82(4):1424–1430, 2012.

[15] Ina M Jürgenliemk-Schulz, Robbert JHA Tersteeg, Judith M Roesink, Stefan Bijmolt, Christel N Nomden, Marinus A Moerland, and Astrid AC de Leeuw. Mri-guided treatment-planning optimisation in intracavitary or combined intracavitary/interstitial pdr brachytherapy using tandem ovoid applicators in locally advanced cervical cancer. *Radiotherapy and Oncology*, 93(2):322–330, 2009.

[16] Akila N Viswanathan, Jennifer Moughan, William Small Jr, Charles Levenback, Revathy Iyer, Sharon Hymes, Adam P Dicker, Brigitte Miller, Beth Erickson, and David K Gaffney. The quality of cervical cancer brachytherapy implantation and the impact on local recurrence and disease-free survival in rtog prospective trials 0116 and 0128. *International journal of gynecological cancer: official journal of the International Gynecological Cancer Society*, 22(1):123, 2012.

[17] Judith Huerta Bahena, Alvaro Martinez, Di Yan, Elizabeth Mele, Gregory Edmunson, Debbie Brown, Maria Hardy, Donald Brabbins, and Gary Gustafson. Spatial reproducibility of the ring and tandem high-dose rate cervix applicator. *International Journal of Radiation Oncology* Biology* Physics*, 41(1):13–19, 1998.

[18] International Organization for Standardization. *Accuracy (trueness and Precision) of Measurement Methods and Results-Part 2: Basic Method for the Determination of Repeatability and Reproducibility of a Standard Measurement Method*. International Organization for Standardization, 1994.

[19] Ferenc Lakosi, Gergely Antal, Csaba Vandulek, Arpad Kovacs, Gabor L Toller, Istvan Rakasz, Gabor Bajzik, Janaki Hadjiev, Peter Bogner, and Imre Repa. Open mr-guided high-dose-rate (hdr) prostate brachytherapy: feasibility and initial experiences open mr-guided high-dose-rate (hdr) prostate brachytherapy. *Pathology & Oncology Research*, 17(2):315–324, 2011.

[20] William Anthony Rutala and David Jay Weber. Guideline for disinfection and sterilization in healthcare facilities, 2008. 2008.

[21] M Skopec. A primer on medical device interactions with magnetic resonance imaging systems. *US Food and Drug Administration (http://www. fda. gov/cdrh/ode/primer16. html), CDRH*, pages 1–16, 1997.

[22] George A Ksander and Palo Alto. Definitions in biomaterials, progress in biomedical engineering, vol. 4. *Annals of Plastic Surgery*, 21(3):291, 1988.

[23] Hsi-Hui Lin, Hsiu-Kuan Lin, I-Hsuan Lin, Yu-Wei Chiou, Horn-Wei Chen, Ching-Yi Liu, Hans I-Chen Harn, Wen-Tai Chiu, Yang-Kao Wang, Meng-Ru Shen, et al. Mechanical phenotype of cancer cells: cell softening and loss of stiffness sensing. *Oncotarget*, 6(25):20946, 2015.

[24] Michigan Gladbeck, Germany Dearborn. Perfactory 4 standard. https://envisiontec.com/wp-content/uploads/2016/09/2017-P4-Standard-Series.pdf. accessed 2017-25-07.

[25] Nina A Mayr, Joseph F Montebello, Joel I Sorosky, Jamie S Daugherty, Dan L Nguyen, George Mardirossian, Jian Z Wang, Susan M Edwards, Wenbin Li, and William TC Yuh. Brachytherapy management of the retroverted uterus using ultrasound-guided implant applicator placement. *Brachytherapy*, 4(1):24–29, 2005.

[26] Richard G Stock, Kenneth Chan, Mitchell Terk, J Keith Dewyngaert, Nelson N Stone, and Peter Dottino. A new technique for performing syed-neblett template interstitial implants for gynecologic malignancies using transrectal-ultrasound guidance. *International Journal of Radiation Oncology* Biology* Physics*, 37(4):819–825, 1997.

[27] Nina A Mayr, E Turgut Tali, WT Yuh, Bruce P Brown, B Chen Wen, Richard E Buller, Barrie Anderson, and David H Hussey. Cervical cancer: application of mr imaging in radiation therapy. *Radiology*, 189(2):601–608, 1993.

[28] Seung Hyup Kim, Byung Ihn Choi, Hyo Pyo Lee, Soon Bum Kang, Young Min Choi, Man Chung Han, and Chu-Wan Kim. Uterine cervical carcinoma: comparison of ct and mr findings. *Radiology*, 175(1):45–51, 1990.

[29] Michael Brodman, Frederick Friedman, Peter Dottino, Cynthia Janus, Steven Plaxe, and Carmel Cohen. A comparative study of computerized tomography, magnetic resonance imaging, and clinical staging for the detection of early cervix cancer. *Gynecologic oncology*, 36(3):409–412, 1990.

[30] Azmat H Sadozye and Nicholas Reed. A review of recent developments in image-guided radiation therapy in cervix cancer. *Current oncology reports*, 14(6):519–526, 2012.

[31] Akila N Viswanathan, Johannes Dimopoulos, Christian Kirisits, Daniel Berger, and Richard Pötter. Computed tomography versus magnetic resonance imaging-based contouring in cervical cancer brachytherapy: results of a prospective trial and preliminary guidelines for standardized contours. *International Journal of Radiation Oncology* Biology* Physics*, 68(2):491–498, 2007.

[32] M Chassang, S Novellas, C Bloch-Marcotte, J Delotte, O Toullalan, A Bongain, and P Chevallier. Utility of vaginal and rectal contrast medium in mri for the detection of deep pelvic endometriosis. *European radiology*, 20(4):1003–1010, 2010.

[33] Michele Larobina and Loredana Murino. Medical image file formats. *Journal of digital imaging*, 27(2):200–206, 2014.

[34] Fabian Rengier, A Mehndiratta, Hendrik von Tengg-Kobligk, Christian M Zechmann, Roland Unterhinninghofen, H-U Kauczor, and Frederik L Giesel. 3d printing based on imaging data: review of medical applications. *International journal of computer assisted radiology and surgery*, 5(4):335–341, 2010.

[35] 3Dhubs. Medical 3d printing application. https://www.3dhubs.com/knowledge-base/medical-3d-printing-applications. accessed 2017-25-06.

[36] Nicolas Magné, Cyrus Chargari, Nicholas SanFilippo, Taha Messai, Alain Gerbaulet, and Christine Haie-Meder. Technical aspects and perspectives of the vaginal mold applicator for brachytherapy of gynecologic malignancies. *Brachytherapy*, 9(3):274–277, 2010.

[37] Søren Haack, Søren Kynde Nielsen, Jacob Christian Lindegaard, John Gelineck, and Kari Tanderup. Applicator reconstruction in mri 3d image-based dose planning of brachytherapy for cervical cancer. *Radiotherapy and Oncology*, 91(2):187–193, 2009.

[38] LE van Heerden, OJ Gurney-Champion, Z van Kesteren, AC Houweling, C Koedooder, CRN Rasch, BR Pieters, and A Bel. Quantification of image distortions on the utrecht interstitial ct/mr brachytherapy applicator at 3t mri. *Brachytherapy*, 15(1):118–126, 2016.

[39] Yuval Ramot, Moran Haim-Zada, Abraham J Domb, and Abraham Nyska. Biocompatibility and safety of pla and its copolymers. *Advanced drug delivery reviews*, 107:153–162, 2016.

[40] C Lee Ventola. Medical applications for 3d printing: current and projected uses. *Pharmacy and Therapeutics*, 39(10):704, 2014.

[41] Nizar N Zein, Ibrahim A Hanouneh, Paul D Bishop, Maggie Samaan, Bijan Eghtesad, Cristiano Quintini, Charles Miller, Lisa Yerian, and Ryan Klatte. Three-dimensional print of a liver for preoperative planning in living donor liver transplantation. *Liver Transplantation*, 19(12):1304–1310, 2013.

[42] Carl Schubert, Mark C Van Langeveld, and Larry A Donoso. Innovations in 3d printing: a 3d overview from optics to organs. *British Journal of Ophthalmology*, 98(2):159–161, 2014.

[43] How is cervical cancer staged? http://www.cancer.org/cancer/cervicalcancer/detailedguide/cervical-cancer-staged. Accessed 2016-11-10.

[44] American Cancer Society. Treatment types. http://www.cancer.org/treatment/treatmentsandsideeffects/ 2016. accessed 7/11/2016.

[45] Zeina Al-Mansour and Claire Verschraegen. Locally advanced cervical cancer: what is the standard of care? *Current opinion in oncology*, 22(5):503–512, 2010.

[46] Bradley J Monk, Michael W Sill, D Scott McMeekin, David E Cohn, Lois M Ramondetta, Cecelia H Boardman, Jo Benda, and David Cella. Phase iii trial of four cisplatin-containing doublet combinations in stage ivb, recurrent, or persistent cervical carcinoma: a gynecologic oncology group study. *Journal of Clinical Oncology*, 27(28):4649–4655, 2009.

[47] 3Dhubs Ben Redwood. Additive manufacturing technologies: An overview. https://www.3dhubs.com/knowledge-base/additive-manufacturing-technologies-overview. accessed 2017-25-06.